International Journal of Applied Mathematics

Volume 38 No. 11s 2025,

ISSN: 1311-1728 (printed version); ISSN: 1314-8060 (on-line version)

MATHEMATICAL MODELING OF A FUZZY LOGIC-BASED CONTROL SYSTEM FOR SUSTAINABLE ENERGY AND ENVIRONMENTAL MANAGEMENT IN INDOOR VERTICAL HYDROPONICS

Analene Montesines Nagayo[1], Mahmood Zayid Al Ajmi[2] and Naga Rama Krishna Guduri[3]

[1,2,3]Electrical, Electronics and Computer Unit, College of Engineering and Technology, University of Technology and Applied Sciences – Al Musanna, Oman

[1]montesines.nagayo@utas.edu.om, [2]mahmood.al-ajmi@utas.edu.om, [3]naga.krishna@utas.edu.om

Abstract

This paper discusses the mathematical modeling and deployment of a fuzzy logic-based control system for sustainable energy and environmental management in an Indoor Vertical Agricultural Production System (IVAPS). The IVAPS consists of four main subsystems: (a) a hydroponic growth tower with vertically stacked mint plants; (b) a solar-powered energy management unit with IoT-based real-time monitoring of battery voltage and inverter output; (c) an environmental control and monitoring module using Particle Photon microcontrollers and sensors to regulate temperature, humidity, and air quality through fuzzy logic; and (d) an IoT-enabled water quality management system that monitors pH, total dissolved solids, electrical conductivity, salinity, and temperature for nutrient recirculation. Energy optimization is accomplished by mathematical formulation of membership functions, rule-based fuzzy inference, and centroid defuzzification to dynamically regulate DC fan speed and environmental actuators. The results showed that the fuzzy logic controller provided an hourly energy saving of 19.5% to 30.8% compared to a conventional ON/OFF controller. Data presented in the interactive mobile application also confirmed that system maintained suitable environmental conditions for mint cultivation in the IVAPS while optimizing energy usage.

Math. Subj. Classification 2020: 03B52, 93C42

Keywords: fuzzy logic control, mathematical modeling, energy optimization, indoor vertical hydroponics, IoT-based monitoring

I. INTRODUCTION

Oman faces food security challenges common to hot, desert-climate countries. These problems arises from four factors: (a) limited freshwater resources, which make it difficult to sustain high levels of agricultural production [1], [2]; (b) lack of crop-producing land, with only approximately 2.2 million hectares suitable for cultivation [2]; (c) high dependency on imported goods, meeting nearly 60% of Oman's food demands according to the Ministry of Agriculture and Fisheries, and increasing the country’s vulnerability to supply chain disruptions and international market price fluctuations [1]; and (d) extreme climatic conditions like heat waves and droughts, which cause significant risks to crops and food stability [3].

Oman is addressing these issues by investing in strategic infrastructure and implementing greenhouse and vertical farming projects to make the country more self-sufficient for food production [4]–[6]. In support of this, an Indoor Vertical Agriculture

Received: August 05, 2025

International Journal of Applied Mathematics
Volume 38 No. 11s 2025,
ISSN: 1311-1728 (printed version); ISSN: 1314-8060 (on-line version)

Production System (IVAPS) was designed and deployed in the electronics workshop classroom of the UTAS–Al Musanna's EE building. The IVAPS prototype, illustrated in Fig. 1, allows plants to grow on vertically stacked shelves in a controlled environment using hydroponics and artificial illumination [7], [8]. Hydroponics, a type of soilless farming, uses water-based solutions rather than soil to deliver nutrients to plants [7]. IVAPS improves crop production per unit area, maximizes available space, and reduces water consumption through closed-loop recirculation in comparison to traditional horizontal greenhouses. This system enables controlled vegetable production in the extreme environment of Oman. When installed indoors, IVAPS can improve air quality by absorbing carbon dioxide (CO_2), reducing total volatile organic compounds (TVOCs), and releasing oxygen [9]–[11]. IVAPS is also suitable for use in indoor settings like classrooms and laboratories since it can help minimize noise by absorbing sound [12].

The IVAPS growth tower integrated the following subsystems to ensure efficient and sustainable operation: (a) a solar-powered energy management module that ran the entire system and provided IoT-based real-time monitoring of battery voltage and inverter output; (b) a Particle Photon-based environmental control and monitoring subsystem, with sensors deployed within the cultivation tower to regulate air temperature (Ta), relative humidity (RH), CO_2 concentration, TVOCs, and indoor lighting (IL) using IoT connectivity and fuzzy logic algorithms. The fuzzy logic control model applied mathematical membership functions, rule-based inference, and centroid defuzzification to dynamically adjust the cooling fans' (CFs) speed, thereby maintaining optimal microclimatic conditions while minimizing energy consumption; (c) a water quality control and monitoring module using Particle Photon microcontrollers, with sensors installed in the cultivation tower to track of pH, total dissolved solids (TDS), electrical conductivity (EC), salinity (SAL), and water temperature (Tw) levels, while managing the recirculation system for efficient water and nutrient delivery; and (d) an interactive mobile application that enabled real-time monitoring, visualization and management of the IVAPS.

Fig. 1. Indoor Vertical Agriculture Production System (IVAPS) prototype

Received: August 05, 2025

International Journal of Applied Mathematics
Volume 38 No. 11s 2025,
ISSN: 1311-1728 (printed version); ISSN: 1314-8060 (on-line version)

Section II of the paper compares several renewable conversion systems, as well as monitoring and control systems used in soilless farming facilities. Section III discusses the design and development of the solar energy management subsystem, monitoring modules, and fuzzy logic control model. Section IV presents data on the performance of the IVAPS modules in monitoring and controlling the air and water quality parameters while reducing the energy needed to operate the prototype. Section V concludes the research work and makes recommendations for possible improvements.

II. RELATED WORKS

The integration of renewable energy conversion systems into soilless agricultural production units, such as aquaponics, aeroponics, and hydroponics, has gained significant attention as a means of sustainable food security measures. Solar, wind, and hybrid systems have been designed to enable continuous operation, optimize energy efficiency, and support actuator-driven processes of soilless farms.

[5] designed a solar-powered aquaponics greenhouse at UTAS-Al Musanna campus, cultivating tilapia and water spinach in a symbiotic environment. The system used an Arduino microcontroller interfaced with sensors that monitored and maintained the greenhouse environmental metrics. The solar power system had two 300 W photovoltaic (PV) panels, four 12 V/ 200 Ah batteries, a 60 A PWM charge controller, and a 1 kW inverter that could provide 4,758 Wh of energy per day. The renewable energy conversion system was able to power the greenhouse system for 24 hours during the winter season, but battery backup lasted only 21.5 hours during summertime under high actuator loads. To address this limitation, [13] proposed an upgraded setup with four 300 W PV panels and eight 12 V/200 Ah batteries. This modification solved the energy shortage during the summer season, enabling uninterrupted 24-hour operation even when evaporative coolers, exhaust fans, and water pumps were all working simultaneously.

In [14], a solar-powered IoT garden fertigation system was designed and implemented using a 150 W PV panel, a PWM charge controller, and a 65 Ah lithium-ion battery. The system provided more than 10 hours of backup power after about 11.5 hours of charging, meeting all energy requirements. [6] designed a hybrid wind–solar energy system for a soilless farm, including a fuzzy inferencing–based decision support model for crop planning. The setup used six 300 W PV panels, a 1 kW wind turbine, and eight 12 V/200 Ah batteries, meeting daily energy needs from 4,380 Wh in winter to 5,920 Wh in summer. The IoT battery monitoring integrated with the system provided continuous and real-time power tracking. [15] described the development of an on-grid solar greenhouse that incorporated machine learning for plant disease detection and automated actuator control. With two 20 W PV panels and a 12 V battery, the system produced 140.16 kWh annually, exceeding the 56.94 kWh/year demand.

Compared to previous research studies, the proposed system introduced a mathematically modeled fuzzy logic controller for dynamic actuator management and integrated IoT-based energy optimization within the IVAPS. The solar power set-up consisted of two 300 W PV panels, four 12 V/200 Ah deep-cycle batteries, a 60 A PWM charge controller, and a 1 kW, 24 V pure sine-wave inverter. Considering approximately 30% losses from wiring, connections, and battery inefficiencies, the solar power system delivered an average of 3,178.8 Wh per day.

In contrast to the approach in [16], where cooling was solely dependent on temperature data, the designed fuzzy logic-based ventilation system mathematically combined the effects of Ta and RH to dynamically regulate the DC fan speed. When compared to traditional ON/OFF controllers, this dual-parameter control significantly improved energy efficiency while maintaining stable microclimatic conditions suitable for mint growth. Furthermore, the integration of IoT and mobile computing technologies enabled real-time monitoring, historical data analysis, and predictive assessment of environmental and water quality parameters. Sensor readings and actuator states were visualized through an interactive mobile application developed using MIT App Inventor and stored on the ThingSpeak cloud and MariaDB database servers. Overall, the system presented an innovative, energy-efficient, and intelligent solution for indoor vertical agriculture.

III. METHODS

A. Design of the sustainable energy management system (SEMS) for the solar-powered indoor vertical agricultural production system (IVAPS)

The IVAPS, with its monitoring and control systems, required a total daily energy of 2,445.2 Wh/day, as derived from the electrical load profile in Table 1. Considering the connection losses and battery inefficiencies of approximately 30%, the adjusted energy requirement was computed as 3,178.8 Wh/day. With an average of 5.5 peak sun hours per day in Oman [17], the solar array was designed to deliver 577.96 W, implemented by connecting two 300 W, 28 V PV modules in parallel, yielding a combined current of 21.43 A. A PWM solar charge controller with a current rating exceeding 26.79 A regulated battery charging and prevented overcharge conditions. The battery bank was set at a 50% depth of discharge (DoD) to extend the lifespan, requiring a minimum capacity of 9,536.4 Wh to ensure 1.5 days of autonomy under low sunlight conditions. The battery storage system was implemented through a series-parallel arrangement of four 12 V, 200 Ah lead-acid batteries. A 1 kW, 24 V pure sinewave inverter converted DC power from the battery bank to AC power, supplying both continuous and peak load demands. Table 2 presents the list of SEMS components and their corresponding specifications.

The IoT-enabled energy meter module employed a PZEM-004T sensor to monitor the AC output voltage of the inverter. Voltage was measured using an internal resistive voltage divider connected across the inverter's live and neutral terminals, while the load current was detected with an external current transformer (CT) clamped around the live conductor [18]. The energy metering IC sampled these signals and calculated real power by multiplying voltage and current, providing accurate readings of voltage, current, and power delivered to the load. These measurements were transmitted to a Particle Photon (PPMC1) microcontroller, which sent the data to the ThingSpeak cloud for real-time monitoring, logging, and remote management, enabling efficient energy use.

International Journal of Applied Mathematics
Volume 38 No. 11s 2025,
ISSN: 1311-1728 (printed version); ISSN: 1314-8060 (on-line version)

Table 1. Electrical load details for the IVAPS with the monitoring and control systems

Electrical Load Details for the IVAPS					
Equipment Name	**Numbe r of Units**	**Powe r (W)**	**Total Powe r (W)**	**Usage Hr/Da y**	**Watt-Hr per Day**
Environmental and Water Quality Monitoring Systems (Particle Photon microcontrollers with sensors)	2	2	4	24	96.0
Environmental and Water Quality Control Systems (Particle Photon microcontrollers with relay and motor drivers)	2	2	4	24	96.0
IoT-based Sustainable Energy Management System (Particle Photon microcontrollers with PZEM-004T and electrical circuits)	2	2	4	24	96.0
Submersible motor pump for WRS	1	25	25	24	600.0
Submersible motor pump for clean water replacement	1	25	25	3	75.0
pH dispenser pump (pH UP or pH DOWN pump)	1	4	4	3	12.0
Nutrients solution pump	1	4	4	1	4.0
Air humidifier (AH)	1	20	20	1	20.0
Exhaust fan (EF)	1	25	25	11	275.0
DC Cooling fans (CFs)	8	1.1	8.8	24	211.2
LED vertical grow lamps (GLs)	2	40	80	12	960.0
Total			**203.8**		**2445.2**

Table 2. SEMS components with specifications

Component	**Specification**
Solar Photovoltaic (PV) panel	2 × 300 W panels (600 W total)
Solar charge controller	PWM controller, 60 A, 12/24 V, max PV input 50 V
Inverter	1000 W / 24 V pure sine wave inverter
Batteries	4 × 12 V, 200 Ah deep cycle

The IoT-based Battery Monitoring Module (IBMM) was implemented using a Particle Photon microcontroller (PPMC2) and a resistive voltage divider to safely monitor the 24 V solar battery bank. The divider circuit scaled down the high battery voltage to a level measurable by the microcontroller's analog input port A0 because its ADC could handle a maximum of 3.3 V. The resistive divider circuit reduced the maximum 32 V battery voltage to 2.91 V by using R1 = 100 kΩ and R2 = 10 kΩ, as shown in (1). The divider output was routed to A0 through a 1 kΩ series resistor to improve reliability. A 10 nF bypass capacitor was connected between A0 and ground for noise suppression. A 3.6 V Zener diode was placed across the same branch to protect the analog input from voltage spikes exceeding the ADC limit. Fig. 2 shows the SEMS circuit diagram, including the solar power conversion, energy meter, and battery monitoring modules, while Fig. 3 presents the actual physical setup of the SEMS.

$$Vmeasured\ by\ PPMC2 = Vbattery * \frac{R2}{(R2+R1)} = 32\ V * \frac{10K\Omega}{110K\Omega} = 2.91\ V \qquad (1)$$

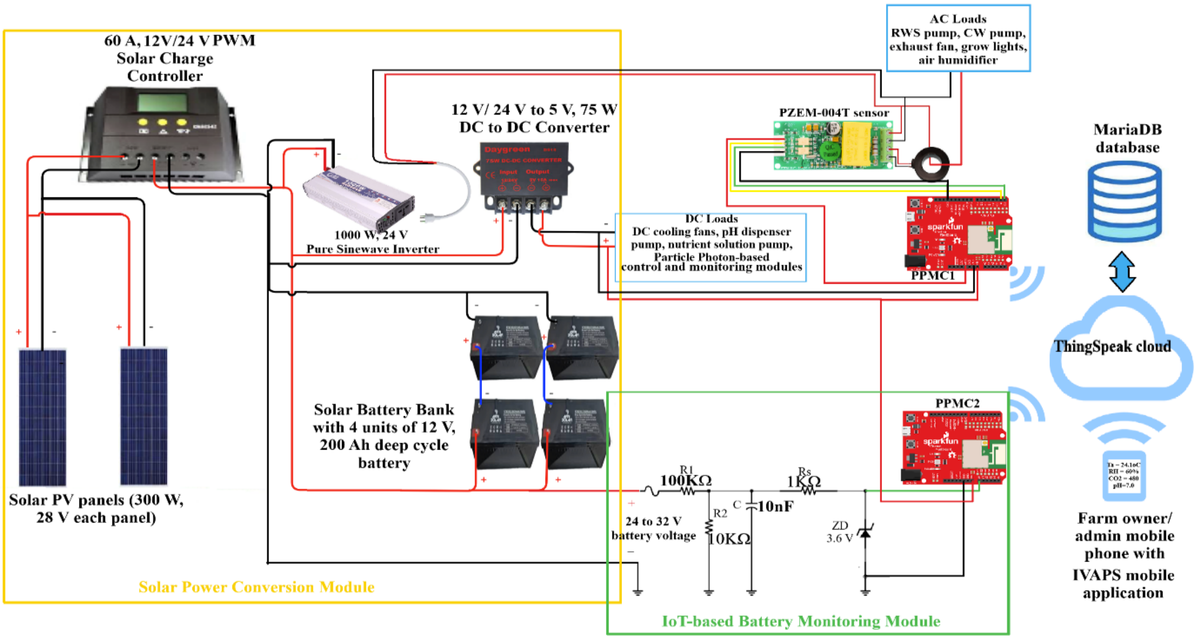

Fig. 2. Circuit diagram of the SEMS with the solar power conversion unit, PZEM-004T energy meter module and battery monitoring module

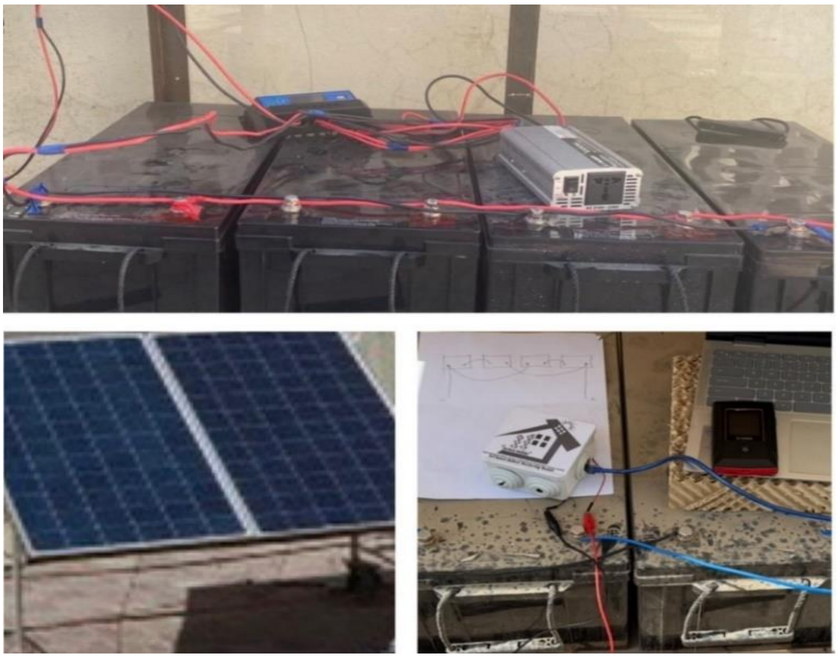

Fig. 3. Actual set-up of the SEMS

International Journal of Applied Mathematics
Volume 38 No. 11s 2025,
ISSN: 1311-1728 (printed version); ISSN: 1314-8060 (on-line version)

B. Design of the Particle Photon-based Environmental Control and Monitoring System for IVAPS

The environmental control and monitoring system for IVAPS was divided into two sub-modules: (a) the Particle Photon-based Environmental and Air Quality Monitoring Subsystem (PPEAQMS), implemented using Photon RedBoard microcontrollers (PPMC3 and PPMC4) and environmental sensors, as shown in Fig. 4; and (b) the Particle Photon-driven Environmental and Air Quality Control Subsystem (PPEAQCS), integrating a Photon RedBoard microcontroller (PPMC5), relay board, L298N motor drivers, and actuators, as illustrated in Fig. 5. The PPEAQMS performed real-time acquisition and processing of environmental and air quality parameters, including Ta, RH, and CO_2 from the SCD41 sensor, total volatile organic compounds (TVOC) from the CCS811 sensor, and illuminance (IL) from an LDR-based photodetector. Target setpoints, operational thresholds, and alert conditions for these parameters were defined based on agronomic recommendations, hydroponics guidelines, and published literature, as summarized in Table 3. The sensor outputs were time-stamped and logged to the ThingSpeak cloud and a MariaDB database for remote monitoring and historical data analysis. The PPEAQCS retrieved the data in the ThingSpeak cloud and applied fuzzy logic-based control to the DC cooling fans (CFs), while activating the exhaust fan (EF), air humidifier (AH), and grow lights (GLs) in real time to maintain the desired environmental and air quality conditions within the IVAPS, as detailed in Table 3.

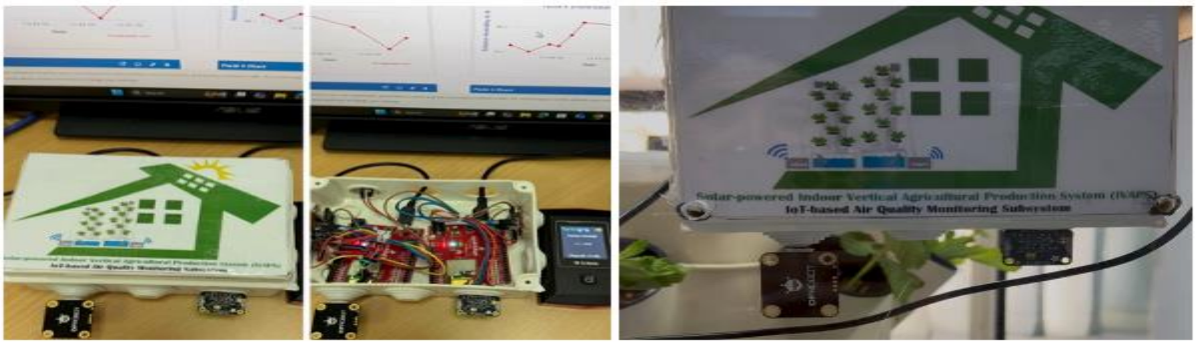

Fig. 4. Particle Photon-based Environmental and Air Quality Monitoring Subsystem (PPEAQMS) prototype

Fig. 5. Particle Photon-driven Environmental and Air Quality Control Subsystem (PPEAQCS) prototype

Table 3. IVAPS Environmental Parameters Optimal Range, Control Actions and Alert Notification Conditions

Parameter	Optimal Range	Control Action (ON / OFF Conditions)	Alert Notification Conditions	References
Air Temperature (Ta)	18–24 °C	CFs at very low speed if 24≥ Ta≥ 18°C; Outside the optimal range, CFs at variable speed based on the fuzzy rules	Ta ≤10°C or Ta ≥ 35°C	[13], [19], [20], [21]
Relative Humidity (RH)	40–70 %	EF ON if RH >70 % until RH returns to normal. AH ON if RH <40 % until RH returns to normal. CFs at very low speed if 40% ≤ RH ≤ 70%; Outside the optimal range, CFs at variable speed based on the fuzzy rules	RH ≤ 25% or RH ≥ 85%	[13], [19], [20], [21]
CO_2 concentration	400–1000 ppm	EF ON if CO_2 >1,000 ppm until CO2 returns to normal	CO_2 < 200 ppm or CO_2 > 1200 ppm	[13], [21], [22]
TVOC	<100 ppb	EF ON if TVOC ≥ 100 ppb until TVOC returns to normal	TVOC ≥ 120 ppb	[23], [24]
Lighting Duration / LDR Voltage	12–16 hours/day; LDR voltage ≥ 4.0 V indicates dark room	GLs ON if LDR voltage ≥ 4.0 V and within scheduled lighting period	GLs OFF ≥ 4.0 V and within scheduled lighting period	[19], [20]

C. Development of the Fuzzy Logic-based DC Cooling Fan Speed Controller Model for IVAPS

The fuzzy logic–based DC cooling fan speed controller (FLCFSCM) was developed as a mathematically modeled control system to regulate ventilation and optimize energy consumption within the IVAPS. The model employed a Mamdani-type fuzzy inferencing system with two input variables, air temperature (Ta) and relative humidity (RH), and one output variable, the cooling fan speed percentage (CFSP), as seen in Fig. 6. Each input variable was defined with practical operating ranges and subdivided into five membership functions (MFs): very low (VL), low (L), normal (NRM), high (H) and very high (VH), resulting in a total of 25 fuzzy rules as expressed in (2). The trapezoidal-shaped MFs for Ta and RH in Figs.

International Journal of Applied Mathematics
Volume 38 No. 11s 2025,
ISSN: 1311-1728 (printed version); ISSN: 1314-8060 (on-line version)
7 and 8 were mathematically configured to satisfy agronomic criteria for optimal transpiration, photosynthesis, and disease prevention. Tables 4 and 5 summarize the fuzzy set parameters and equations for Ta and RH. The trapezoidal MF plots exhibited flat-top regions, which enhanced the model's robustness to minor input variations and reduced computational complexity while maintaining interpretability and effective control performance [25][26].

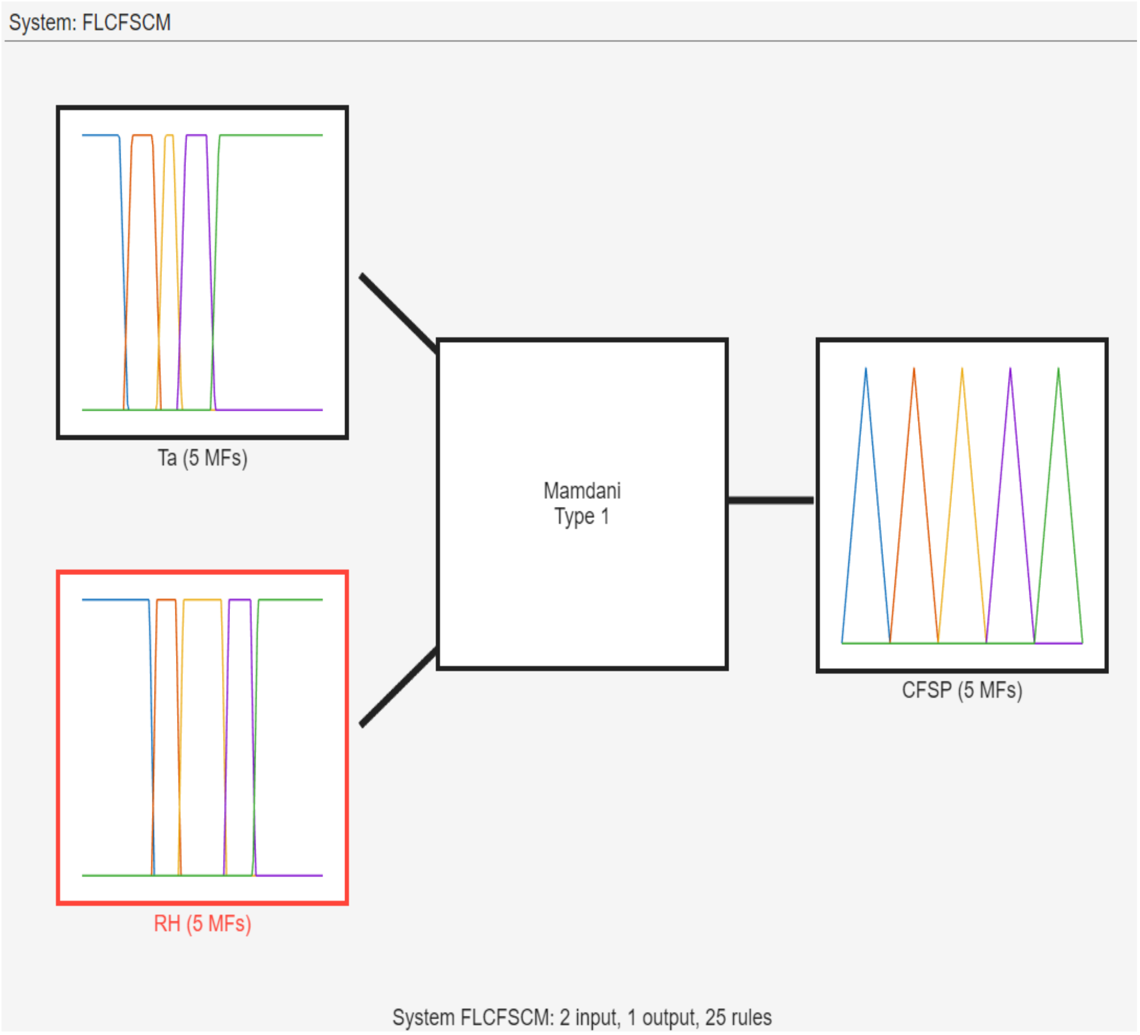

Fig. 6. Block diagram of the FLCFSCM for IVAPS

$$nFR = MF_{Ta} \text{ x } MF_{RH} = 5 \text{ x } 5 = 25 \text{ rules} \quad (2)$$

Where:
nFR = number of fuzzy rules for FLCFSCM
MF_{Ta}= number of membership functions for Ta
MF_{RH} = number of membership functions for RH

Fig. 9 shows the triangular-patterned MF plots for cooling fan speed output percentage (CFSP) that defined five intensity levels: very low speed (VLS), low speed (LS), moderate speed (MS), high speed (HS), and very high speed (VHS). Triangular MFs for actuator control provided an effective trade-off between control precision and computational simplicity [26]. Table 6 describes the fuzzy sets, associated parameters, and MF equations for CFSP, providing a clear mathematical framework for executing energy-efficient ventilation management within the IVAPS.

International Journal of Applied Mathematics
Volume 38 No. 11s 2025,
ISSN: 1311-1728 (printed version); ISSN: 1314-8060 (on-line version)

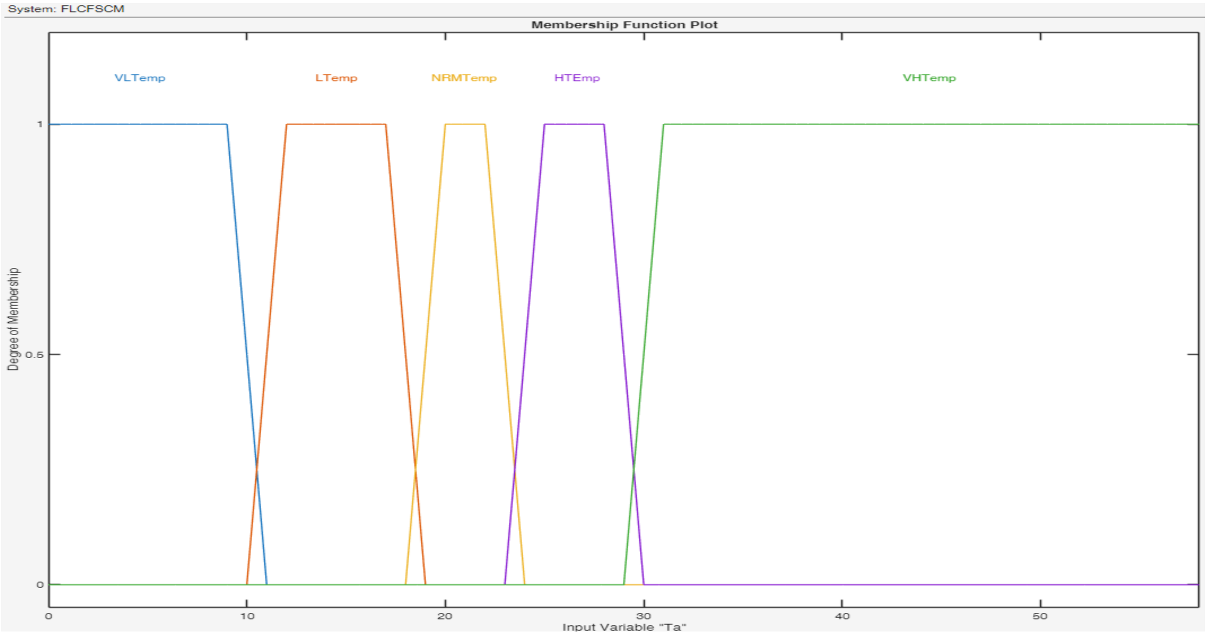

Fig. 7. Trapezoidal-shaped MF plot for Ta

Table 4. The fuzzy sets, parameters and equations of the trapezoidal-shaped MF for Ta

Fuzzy Input Variable	Fuzzy Sets	Trpmf parameters	Trapezoidal Membership Functions
Ta	VLTemp	[0, 0, 9, 11]	$\mu_{VLTemp}(Ta) = \begin{cases} 1 \text{ if } Ta \leq 9 \\ (11 - Ta) / (11 - 9) \text{ if } 9 < Ta \leq 11 \\ 0 \text{ if } Ta > 11 \end{cases}$ (3)
	LTemp	[10, 12, 17, 19]	$\mu_{LTemp}(Ta) = \begin{cases} 0 \text{ if } Ta < 10 \text{ or } Ta > 19 \\ (Ta - 10) / (12 - 10) \text{ if } 10 \leq Ta < 12 \\ 1 \text{ if } 12 \leq Ta \leq 17 \\ (19 - Ta) / (19 - 17) \text{ if } 17 < Ta \leq 19 \end{cases}$ (4)
	NRMTemp	[18, 20, 22, 24]	$\mu_{NRMTemp}(Ta) = \begin{cases} 0 \text{ if } Ta < 18 \text{ or } Ta > 24 \\ (Ta - 18) / (20 - 18) \text{ if } 18 \leq Ta < 20 \\ 1 \text{ if } 20 \leq Ta \leq 22 \\ (24 - Ta) / (24 - 22) \text{ if } 22 < Ta \leq 24 \end{cases}$ (5)
	HTemp	[23, 25, 28, 30]	$\mu_{HTemp}(Ta) = \begin{cases} 0 \text{ if } Ta < 23 \text{ or } Ta > 30 \\ (Ta - 23) / (25 - 23) \text{ if } 23 \leq Ta < 25 \\ 1 \text{ if } 25 \leq Ta \leq 28 \\ (30 - Ta) / (30 - 28) \text{ if } 28 < Ta \leq 30 \end{cases}$ (6)

	VHTemp	[29, 31, 58, 58]	$\mu_{VHTemp}(Ta) =$ { 0 if Ta < 29 (Ta – 29) / (31 – 29) if 29 ≤ Ta < 31 1 if Ta ≥ 31	(7)

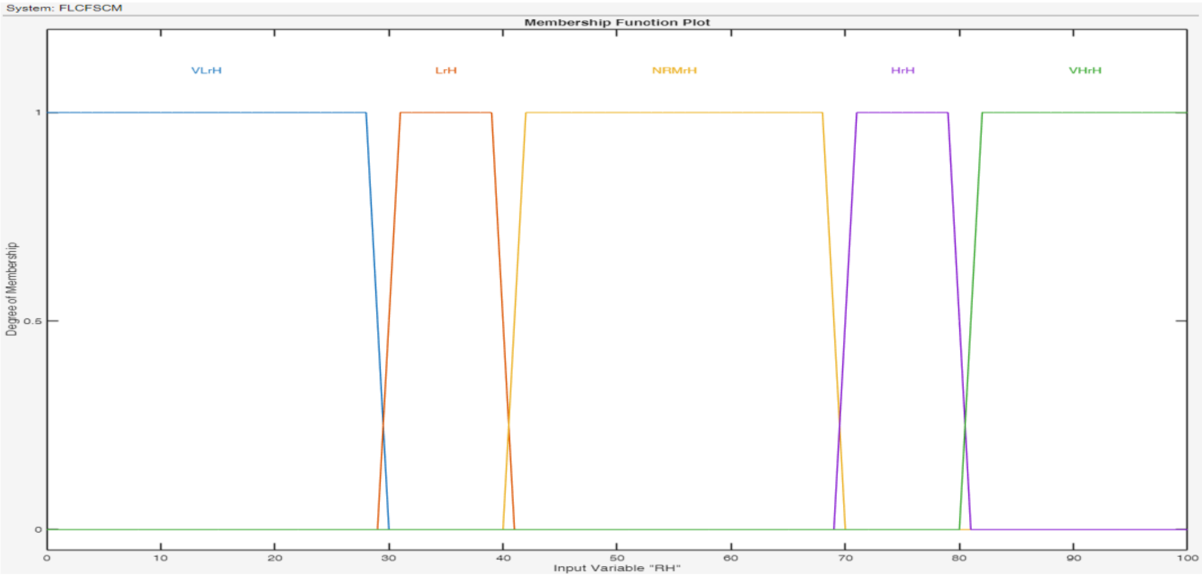

Fig. 8. Trapezoidal-shaped MF plot for RH

Table 5. The fuzzy sets, parameters and equations of the trapezoidal-shaped MF for RH

Fuzzy Input Variable	Fuzzy Sets	Trpmf parameters	Trapezoidal Membership Functions	
RH	VLrH	[0, 0, 28, 30]	$\mu_{VLrH}(RH)=$ { 1 if RH ≤ 28 (30 – RH) / (30 – 28) if 28 < RH≤ 30 0 if RA > 30	(8)
	LrH	[29, 31, 39, 41]	$\mu_{LrH}(RH) =$ { 0 if RH < 29 or RH > 41 (RH – 29) / (31 – 29) if 29 ≤ RH < 31 1 if 31 ≤ RH ≤ 39 (41 – RH) / (41 – 39) if 39 < Ta ≤ 41	(9)
	NRMrH	[40, 42, 68, 70]	$\mu_{NRMrH}(RH) =$ { 0 if RH < 40 or RH > 70 (RH – 40) / (42 – 40) if 40 ≤ RH < 42 1 if 42 ≤ Ta ≤ 68 (70 – RH) / (70 –68) if 68 < RH ≤ 70	(10)
	HrH	[69, 71, 79, 81]	$\mu_{HrH}(RH) =$ { 0 if RH < 69 or RH > 81 (RH – 69) / (71 – 69) if 69 ≤ RH < 71 1 if 71 ≤ RH ≤ 79	(11)

International Journal of Applied Mathematics
Volume 38 No. 11s 2025,
ISSN: 1311-1728 (printed version); ISSN: 1314-8060 (on-line version)

			(81 – RH) / (81 – 79) if 79 < RH ≤ 81	
	VHrH	[80, 82, 100, 100]	$\mu_{VHrH}(RH) =$ { *0 if RH < 80* *(RH – 80) / (82 – 80) if 80 ≤ RH < 82* *1 if RH ≥ 82*	(12)

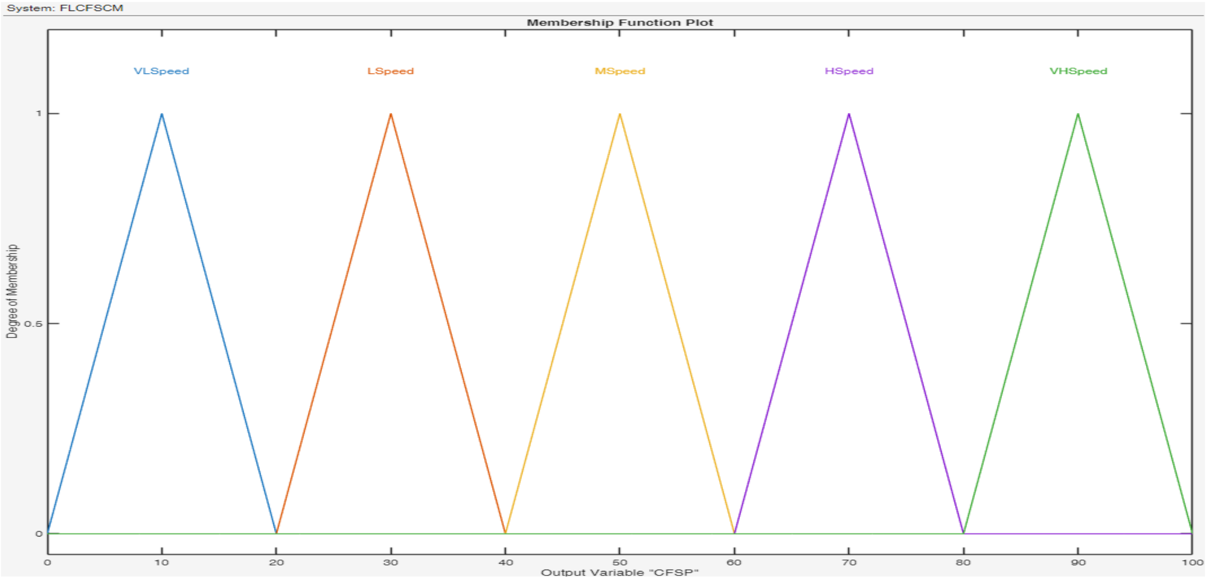

Fig. 9. Triangular-patterned MF plot for CFSP

Table 6. The fuzzy sets, parameters and equations of the triangular-patterned MFs for CFSP

Fuzzy Output Variable	**Fuzzy Sets**	**Trimf parameters**	**Triangular Membership Functions**	
CFSP	VLSpeed	[0, 10, 20]	$\mu_{VLSpeed}(CFSP) =$ { *0 if CFSP ≤ 0* *(CFSP - 0) / (10 - 0) if 0 < CFSP ≤ 10* *(20 - CFSP) / (20– 10) if 10 < CFSP ≤ 20* *0 if CFSP > 20*	(13)
	LSpeed	[20, 30, 40]	$\mu_{LSpeed}(CFSP) =$ { *0 if CFSP ≤ 20* *(CFSP – 20) / (30 – 20) if 20 < CFSP ≤ 30* *(40 - CFSP) / (40 – 30) if 30 < CFSP ≤ 40* *0 if CFSP > 40*	(14)
	MSpeed	[40, 50, 60]	{ *0 if CFSP ≤ 40* *(CFSP – 40) / (50 – 40)*	

ISSN: 1311-1728 (printed version); ISSN: 1314-8060 (on-line version)

			$\mu_{MSpeed}(CFSP) =$	*if* $40 < CFSP \leq 50$ $(60 - CFSP) / (60 - 50)$ *if* $50 < CFSP \leq 60$ 0 *if* $CFSP > 60$	(15)
	HSpeed	[60, 70, 80]	$\mu_{HSpeed}(CFSP) =$	{ 0 *if* $CFSP \leq 60$ $(CFSP - 60) / (70 - 60)$ *if* $60 < CFSP \leq 70$ $(80 - CFSP) / (80 - 70)$ *if* $70 < CFSP \leq 80$ 0 *if* $CFSP > 80$	(16)
	VHSpeed	[80, 90, 100]	$\mu_{VHSpeed}(CFSP) =$	{ 0 *if* $CFSP \leq 80$ $(CFSP - 80) / (90 - 80)$ *if* $80 < CFSP \leq 90$ $(100 - CFSP) / (100 - 90)$ *if* $90 < CFSP \leq 100$ 0 *if* $CFSP > 100$	(17)

The FLCFSCM used the 25 fuzzy rules shown in Fig. 10 to determine an appropriate CFSP by mapping all possible combinations of Ta and RH. By using minimum operators for both logical conjunction (AND) and implication, the inference process ensured that the weakest condition controlled the rule activation strength, preserving system stability and avoiding fan speed overcorrection. To compute the final crisp CFSP with accuracy and smoothness, centroid defuzzification was used. The centroid defuzzification equation for FLCFSCM is presented in (18). This mathematical modeling approach enabled dynamic, energy-efficient ventilation control, contributing to the overall sustainability of the indoor hydroponic system.

	Rule
1	If Ta is VLTemp and RH is VLrH then CFSP is VLSpeed
2	If Ta is LTemp and RH is VLrH then CFSP is VLSpeed
3	If Ta is NRMTemp and RH is VLrH then CFSP is LSpeed
4	If Ta is HTEmp and RH is VLrH then CFSP is MSpeed
5	If Ta is VHTemp and RH is VLrH then CFSP is HSpeed
6	If Ta is VLTemp and RH is LrH then CFSP is VLSpeed
7	If Ta is LTemp and RH is LrH then CFSP is LSpeed
8	If Ta is NRMTemp and RH is LrH then CFSP is LSpeed
9	If Ta is HTEmp and RH is LrH then CFSP is MSpeed
10	If Ta is VHTemp and RH is LrH then CFSP is HSpeed
11	If Ta is VLTemp and RH is NRMrH then CFSP is VLSpeed
12	If Ta is LTemp and RH is NRMrH then CFSP is LSpeed
13	If Ta is NRMTemp and RH is NRMrH then CFSP is VLSpeed
14	If Ta is HTEmp and RH is NRMrH then CFSP is MSpeed
15	If Ta is VHTemp and RH is NRMrH then CFSP is HSpeed
16	If Ta is VLTemp and RH is HrH then CFSP is LSpeed
17	If Ta is LTemp and RH is HrH then CFSP is MSpeed
18	If Ta is NRMTemp and RH is HrH then CFSP is MSpeed
19	If Ta is HTEmp and RH is HrH then CFSP is HSpeed
20	If Ta is VHTemp and RH is HrH then CFSP is VHSpeed
21	If Ta is VLTemp and RH is VHrH then CFSP is MSpeed
22	If Ta is LTemp and RH is VHrH then CFSP is MSpeed
23	If Ta is NRMTemp and RH is VHrH then CFSP is HSpeed
24	If Ta is HTEmp and RH is VHrH then CFSP is VHSpeed
25	If Ta is VHTemp and RH is VHrH then CFSP is VHSpeed

Fig. 10. Fuzzy rules for the FLCFSCM

International Journal of Applied Mathematics
Volume 38 No. 11s 2025,
ISSN: 1311-1728 (printed version); ISSN: 1314-8060 (on-line version)

$$\boldsymbol{CFSP'} = \frac{\sum_{k=1}^{n} \mu_{A(CFSP_k)} * CFSP_k}{\sum_{k=1}^{n} \mu_{A(CFSP_k)}} \qquad (18)$$

Where:
CFSP' = final crisp CF speed percentage.
$CFSP_k$ = discrete points of CFSP, ranging from 0 to 100%.
$\mu_{A(CFSPk)}$ = aggregated membership value of the fuzzy output at $CFSP_k$,after applying all the fuzzy rules
n = total number of discrete points in the CFSP output.

D. Design of the Particle Photon-based Water Quality Control and Monitoring System for IVAPS

The water quality control and monitoring system for IVAPS was composed of two sub-modules: (a) the IoT-enabled Water Quality Monitoring Subsystem (PPWQMS), implemented using Particle Photon microcontrollers (PPMC6 and PPMC7), a DS18B20 water temperature sensor, and Atlas-Scientific pH and conductivity sensors; and (b) the IoT-based Water Quality Control Subsystem (PPWQCS), which integrated a Particle Photon microcontroller (PPMC8), relay driver, and actuators, as illustrated in Fig. 11. The PPWQMS acquired and processed pH, EC, TDS, SAL, and Tw in real time. Operational thresholds, control actions, and alert conditions for these parameters were defined based on agronomic recommendations, hydroponics guidelines, and published literature, as summarized in Table 7. Sensor-read data were time-stamped and stored in the ThingSpeak cloud and a MariaDB database for remote monitoring and data management. To maintain optimal water quality for IVAPS, the PPWQCS automatically activated the pH dispenser pump and the clean water (CW) pump when necessary based on real-time data obtained from the ThingSpeak cloud. The nutrient solution (NS) pump operated on a nightly basis, synchronized with the photoperiod established by the GLs. This timing ensured that plants absorbed nutrients during the active photosynthetic phase.

Table 7. IVAPS Water Quality Parameters Optimal Range, Control Actions and Alert Notification Conditions

Parameter	**Optimal Range**	**Control Action (ON / OFF Conditions)**	**Alert Notification Conditions**	**References**
pH level	5.5–7.0	CW pump and pH DOWN dispenser pump ON if pH >7.0 until pH returns to normal level CW pump and pH UP dispenser pump ON if pH <5.5 until pH returns to normal level	pH < 5.0 or pH > 8.0	[19], [21], [27], [28], [29]
Water temperature (Tw)	20–25 °C	If Tw >25 °C or <20 °C, CW pump ON until Tw returns to normal	Tw < 12 °C or Tw > 35 °C	[13], [30]

Received: August 05, 2025

International Journal of Applied Mathematics
Volume 38 No. 11s 2025,
ISSN: 1311-1728 (printed version); ISSN: 1314-8060 (on-line version)

Electrical Conductivity (EC)	1,500 - 2,500 µS/cm	CW pump ON if EC > 2,500 µS/cm until EC returns to normal	EC > 3,000 µS/cm	[19], [30]–[33]
Total Dissolve Solids (TDS)	750 - 1250 ppm; TDS is approximately 50% to 65% of EC [32],[33]	CW pump ON if TDS > 1,250 ppm until returns to normal	TDS > 1500 ppm	[31]–[33]
Salinity (SAL)	≤2.0 ppt	CW pump ON if SAL > 2.0 until SAL returns to normal	SAL >2.0 ppt	[13], [34]

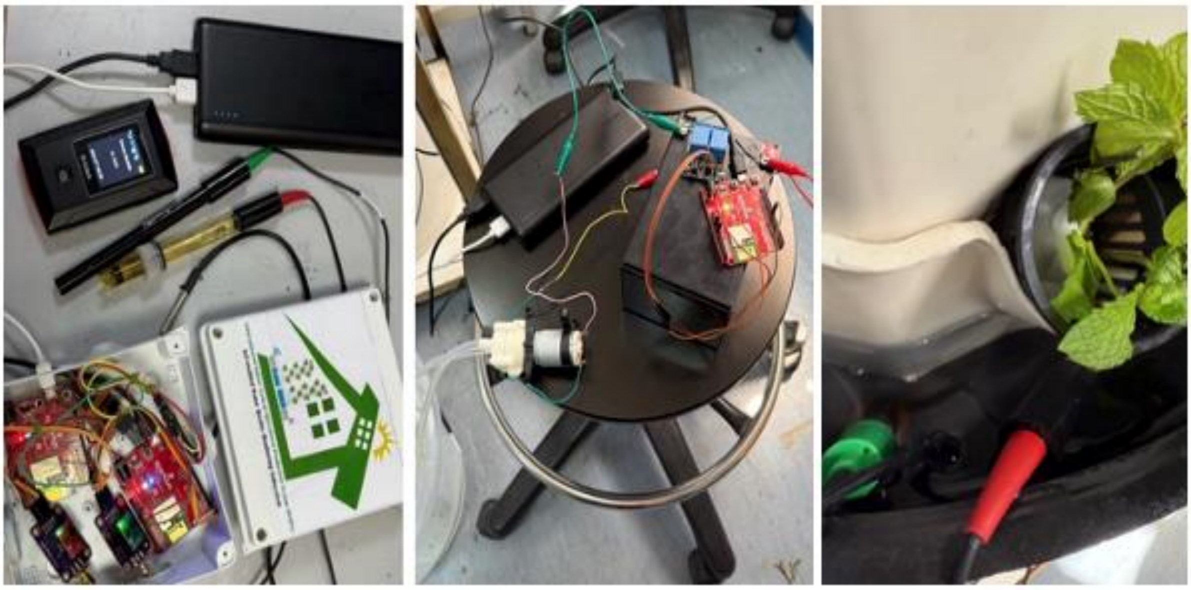

Fig. 11. Particle Photon-based Water Quality Control and Monitoring System for IVAPS

E. Interactive Mobile Application Design for Monitoring and Management of IVAPS (MAIVAPS)

The interactive mobile application for the Indoor Vertical Agriculture Production System (MAIVAPS) was developed using MIT App Inventor to monitoring and manage the IVAPS activities. MAIVAPS connected with the IoT-enabled monitoring modules using RESTful APIs. A PHP middleware layer managed client requests, processed incoming data, and secured all communication with the MariaDB database, supporting real-time dashboards, historical data visualization, and threshold-based alerts.

The MAIVAPS landing screen in Fig. 12(a) introduced the system and provided access to user registration and secure login. As shown in Fig. 12(b), the login screen verified the user's credentials to protect system data. Successful logins proceeded to the main dashboard, while incorrect entries returned the user to the landing screen. Fig. 12(c) shows the main dashboard with interactive buttons to access environmental and water quality data, track actuator status, monitor the SEMS parameters, and receive critical alerts.

International Journal of Applied Mathematics
Volume 38 No. 11s 2025,
ISSN: 1311-1728 (printed version); ISSN: 1314-8060 (on-line version)

The MAIVAPS included a rule-based explainable AI (XAI) feature that helps users understand how the FLCFSCM makes decisions. It also utilized natural language processing (NLP) through MIT App Inventor's text-to-speech (TTS) toolbox to provide real-time verbal guidance to users, report environmental and water quality data, and communicate actuator status. These features enhanced the MAIVAPS's usability and interaction with the users.

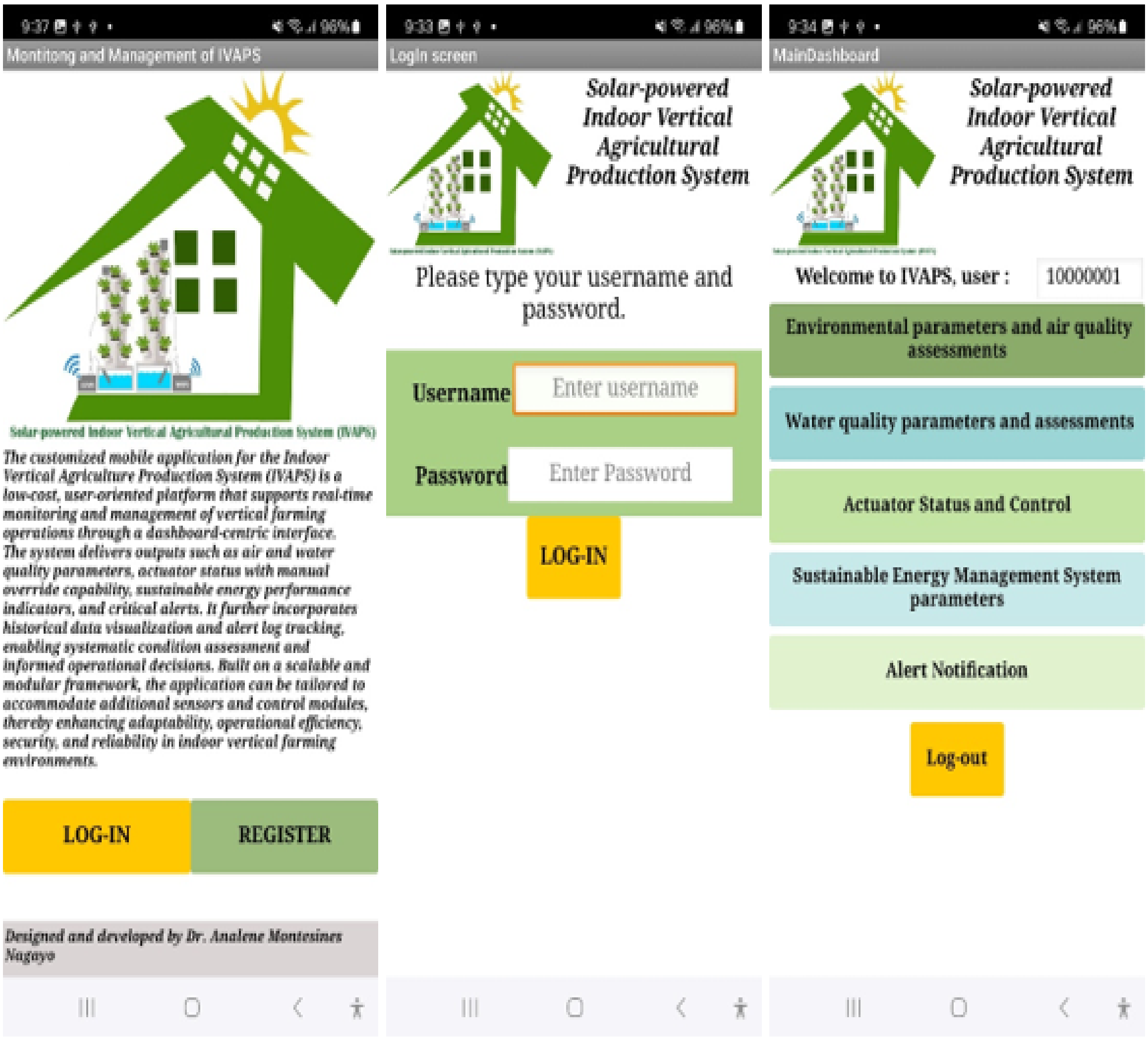

(a) (b) (c)

Fig. 12. User interface of the MAIVAPS: (a) landing screen, (b) log-in screen and (c) main dashboard

IV. RESULTS AND DISCUSSION

A. Results and Discussion for the Sustainable Energy Management System (SEMS)

In the preliminary testing, the PZEM004T energy meter module was calibrated using a laboratory-grade digital multimeter and wattmeter to guarantee accurate voltage and power measurements. The inverter's AC output voltage varied between 230 and 241 V, which is still

Volume 38 No. 11s 2025,
ISSN: 1311-1728 (printed version); ISSN: 1314-8060 (on-line version)

within the manufacturer's specified ±5% tolerance of the nominal 210 to 230 V output. The inverter output voltage was uploaded to the ThingSpeak cloud and saved in the database, as illustrated in Fig. 13.

The calibrated module was used for subsequent load characterization. As illustrated in Fig. 14, the energy meter recorded a baseline consumption of 1.4 W while all actuators were deactivated. As shown in Figs. 15(a) and 15(b), the WRS pump consumed 24.5 W while the CW pump ran at 22.6 W. Figures 16(a) and 16(b) demonstrate that the AH operated with an average power consumption of 18.2 W and the EF used about 23.8 W of power. According to Fig. 17(a), each GL panel demanded 39.9 W, resulting in a combined load of 79.8 W for dual-panel operation. The DC CFs deployed in the IVAPS demonstrated a rated consumption of 1.1 W per unit at full speed, as depicted in Fig. 17(b). With a configuration of two CFs per side, totaling eight CFs in the growth chamber, the maximum airflow power requirement was quantified as 8.8 W. The pH dispenser and nutrient solution pumps each added 4 W to the overall system load.

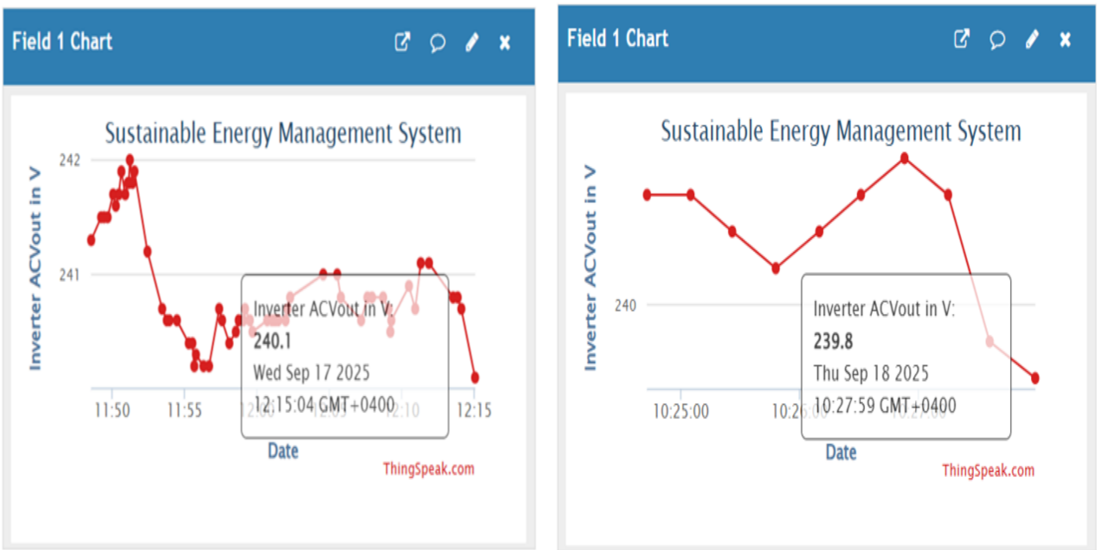

Fig. 13. Sample Inverter AC output voltage as displayed in the ThingSpeak cloud

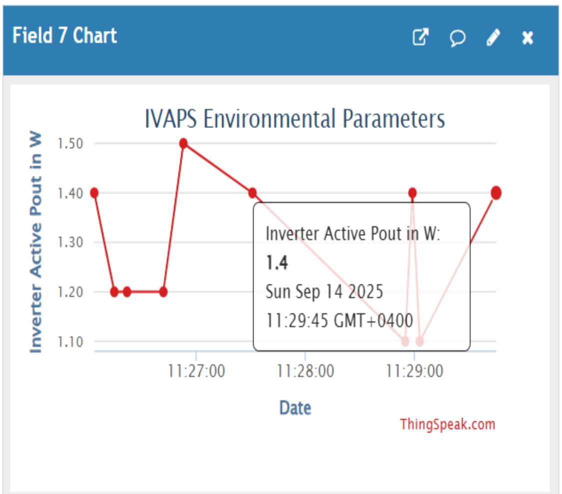

Fig. 14. IoT-based PZEM-004T Energy Meter power drawn from the inverter with all actuators OFF

Received: August 05, 2025

ISSN: 1311-1728 (printed version); ISSN: 1314-8060 (on-line version)

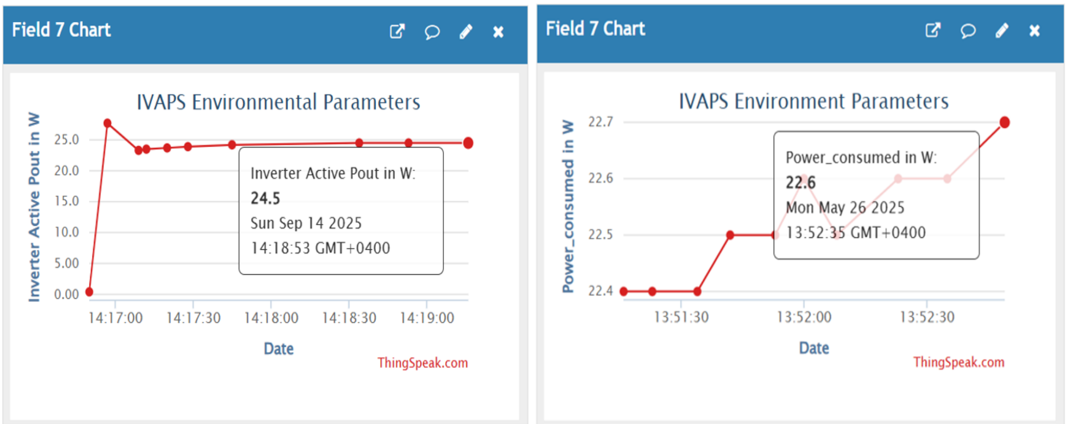

(a) (b)

Fig. 15. Power drawn by (a) WRS pump and (b) CW pump from the inverter

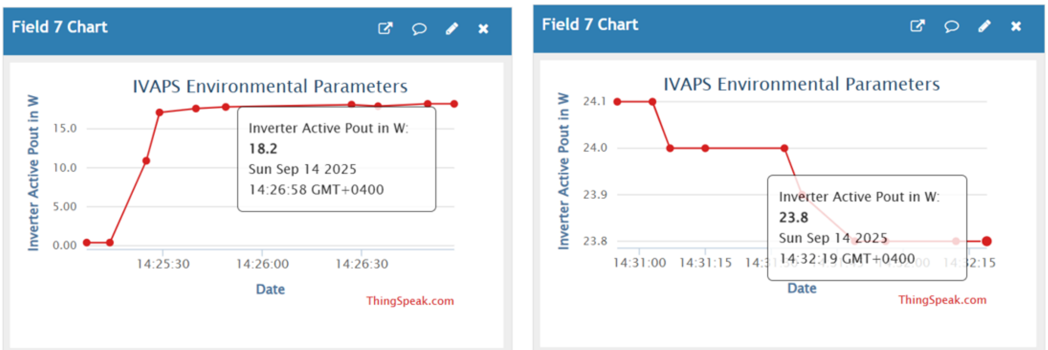

(a) (b)

Fig. 16. Power drawn by the (a) AH and (b) EF from the inverter

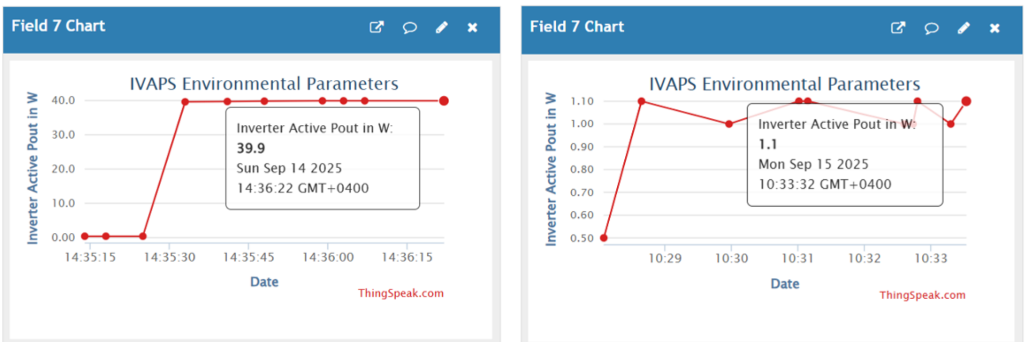

(a) (b)

Fig. 17. Power drawn by (a) one vertical GL panel and (b) one CF from the inverter

Under high-RH conditions, with all other parameters within normal operating ranges, the WRS pump was ON, the EF was ON, the CFs operated at medium speed, and all control and monitoring subsystems were active. In this state, the system consumed 62.6 W, as shown in Fig. 18(a), corresponding to approximately 6.26% of the 1000 W inverter capacity. Under normal environmental and water-quality conditions, with the WRS pump operating, the very-low-speed CFs engaged, and all control and monitoring subsystems active, the system consumed 36.4 W, as shown in Fig. 18(b), corresponding to approximately 3.64% of the

Received: August 05, 2025

ISSN: 1311-1728 (printed version); ISSN: 1314-8060 (on-line version)

inverter capacity. These results demonstrate a substantial margin for safe and efficient operation.

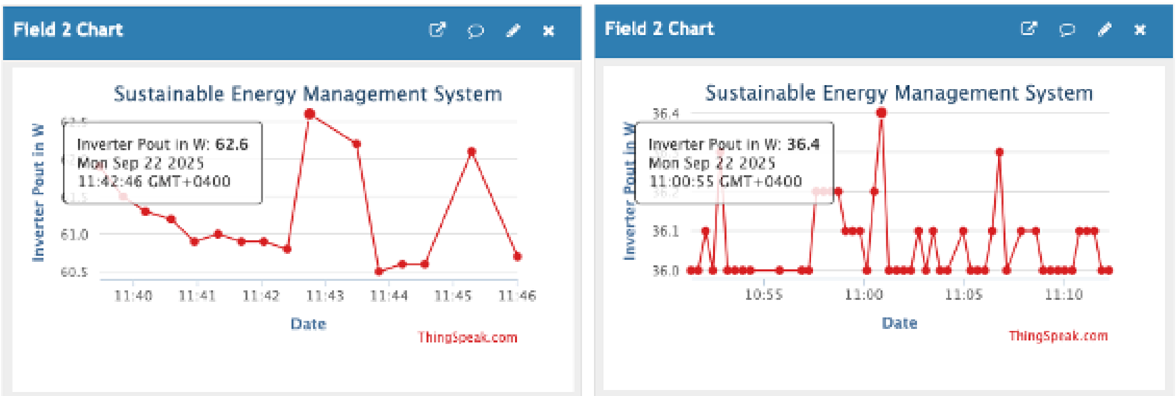

(a) (b)

Fig. 18. Total power drawn from the inverter under (a) high RH condition with all other parameter within normal operating ranges, and (b) normal environmental condition

According to Fig. 19, the IBMM supplied a battery voltage between 25.6 V and 27.1 V over a 24-hour duration, with an average of 26.6 V to operate the IVAPS. This indicates a continuous battery charge-discharge cycle. The lowest voltage of 25.6 V was recorded between 4:00 and 5:00 in the morning while the GL and CFs were running all the time. Solar charging began at 06:00 to 07:00 with a charge of 25.8 V and reached a maximum of 27.1 V during peak solar hours from 09:00 to 15:00.

During 18:00 to 22:00, simultaneous EF, CFs, GL, and WRS pump operation caused a voltage drop from 26.7 V to 26.2 V, remaining within safe limits. Overall, the SEMS maintained voltages within ± 5% of the nominal 26.5 V, ensuring balanced energy consumption and battery protection.

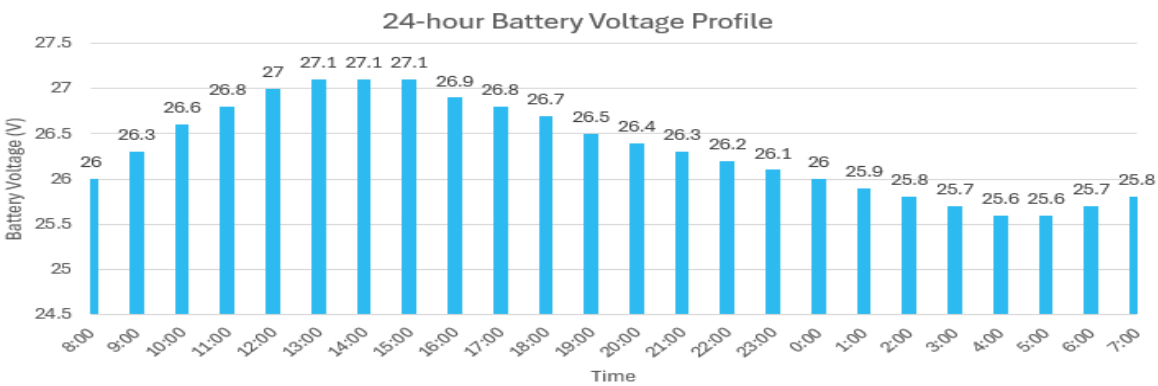

Fig. 19. 24-hour Battery Voltage Profile from the IBMM

B. Results and Discussion for the Particle Photon-based Environmental Control and Monitoring System of the IVAPS

International Journal of Applied Mathematics
Volume 38 No. 11s 2025,
ISSN: 1311-1728 (printed version); ISSN: 1314-8060 (on-line version)

(a) (b) (c)

Fig. 20. PPEAQMS calibration against INKBIRD Plus air quality detector

The PPEAQMS sensors were calibrated using two commercial air quality detectors, INKBIRD Plus and VOCOO, before being used in the IVAPS. As shown in Fig. 20(a), the Ta readings from VOCOO and PPEAQMS were 24.5°C and 24.73°C, giving an absolute percent difference of 0.934%. For RH, Fig. 20(b) shows values of 45% from the VOCOO and 45.45% from the PPEAQMS. This corresponds to an absolute percentage difference of 0.995%. The CO_2 measurements, shown in Fig. 20(c), were 406 ppm for the INKBIRD Plus and 405 ppm for the PPEAQMS, with an absolute percent difference of 0.247%. The results show that the environmental and air quality data collected by the PPEAQMS are comparable to those from commercial air quality monitors. This confirms the system's acceptability for usage in the IVAPS chamber.

Table 8 presents the weekly average 24-hour IVAPS data, collected in the electronics workshop classroom (EE101) using the Particle Photon–based monitoring and control system (PPEAQMS and PPEAQCS). Ta fluctuated between 20.6°C at 09:00 and 28.5°C at 01:00. The lowest temperatures were observed throughout the morning while the centralized air conditioning (AC) was active. On the other hand, the highest temperatures were observed after the AC was turned off at 18:00, which was accompanied with the continuous operation of the GLs. RH changed from 58.9% at 09:00 to 71.5% at 21:00. The continuously running WRS kept the RH stable at its baseline level. Since RH remained above 40% for 24 hours, the AH stayed off throughout the observation period. The observed data trends are comparable with the results in [35], which emphasized the need for precise Ta and RH control in small-scale indoor plant growth environments.

CO_2 concentrations varied based on the classroom occupancy. The level increased from 577 ppm at 08:00 to a peak level of 1030 ppm at 13:00 during the busiest classroom hours, then decreased gradually to 546 ppm at 05:00 when the classroom was unoccupied. The overnight

International Journal of Applied Mathematics
Volume 38 No. 11s 2025,
ISSN: 1311-1728 (printed version); ISSN: 1314-8060 (on-line version)

reduction of about 30 to 40 ppm was due to plant photosynthesis, supported by artificial GLs operating from 18:00 to 07:00. TVOC concentrations ranged from 2 ppb at 08:00 to 24 ppb at 23:00. Daytime values remained below 22 ppb, indicating minimal emissions from laboratory activities. Slight increases in TVOC values were observed at night due to the accumulation of plant- and material-related volatiles in the closed environment. The results align with the findings in [36], which showed that elevated CO_2 levels can influence metabolic activity in mint and similar plant species, affecting VOC release and photosynthesis.

The CF speeds were managed by a fuzzy logic controller that used Ta and RH as its inputs. During low-load periods, such as 08:00 to 09:00 and 15:00 to 17:00, the controller kept the CFSP at VLS setting. From 21:00 to midnight, when both Ta and RH readings were elevated, the controller shifted the CFSP to HS. At 14:00, both Ta and RH were still within the acceptable range, but RH was getting close to the upper limit. Instead of keeping the CFs at the VLS setting, the fuzzy logic controller raised them to LS, showing that it reacts early when conditions start nearing the threshold. A similar adjustment occurred at 18:00, when Ta began approaching its upper threshold. The controller again set the CFs at LS to ensure proactive reduction of thermal load before peak nighttime values were reached. These adjustments demonstrate how the fuzzy logic controller works to balance energy efficiency and environmental stability. The EF activated when CO_2 or RH levels exceeded the threshold values, particularly between 11:00-13:00 and 20:00-midnight. The LDR detected external light intensity, with 0 V corresponding to daytime brightness and 4.8 V indicating darkness, enabling synchronized GL operation to sustain mint photosynthetic activity during non-daylight hours.

Table 8. Sample weekly average 24-hour environmental data and actuator status for the IVAPS

Time	Environmental Parameter Readings					Actuator status and controlled action					Occupants
	Ta (°C)	RH (%)	CO_2 (ppm)	TVOC (ppb)	LDR Vo (V)	WRS pump status	EF status	CFs Speed	GLs Status	AH Status	
8:00	21.4	61.0	577	2	0	ON	OFF	VLS	OFF	OFF	<10
9:00	20.6	58.9	679	3	0	ON	OFF	VLS	OFF	OFF	<10
10:00	22.0	67.5	703	7	0	ON	OFF	VLS	OFF	OFF	20 to 25
11:00	22.6	71.2	810	15	0	ON	ON	MS	OFF	OFF	20 to 25
12:00	22.9	70.8	954	20	0	ON	ON	MS	OFF	OFF	20 to 25

International Journal of Applied Mathematics
Volume 38 No. 11s 2025,
ISSN: 1311-1728 (printed version); ISSN: 1314-8060 (on-line version)

13:00	22.5	70.3	1030	22	0	ON	ON	MS	OFF	OFF	20 to 25
14:00	22.0	69.3	743	19	0	ON	OFF	LS	OFF	OFF	15 to 20
15:00	21.9	67.8	737	17	0	ON	OFF	VLS	OFF	OFF	15 to 20
16:00	21.8	65.9	701	10	0	ON	OFF	VLS	OFF	OFF	10 to 15
17:00	21.7	64.2	655	8	0	ON	OFF	VLS	OFF	OFF	10 to 15
18:00	23.6	68.3	639	14	4.8	ON	OFF	LS	ON	OFF	0
19:00	24.8	69.4	622	15	4.8	ON	OFF	MS	ON	OFF	0
20:00	25.7	70.8	612	18	4.8	ON	ON	HS	ON	OFF	0
21:00	26.6	71.5	606	20	4.8	ON	ON	HS	ON	OFF	0
22:00	27.3	71.2	598	23	4.8	ON	ON	HS	ON	OFF	0
23:00	27.8	70.9	590	24	4.8	ON	ON	HS	ON	OFF	0
0:00	28.2	70.1	586	23	4.8	ON	ON	HS	ON	OFF	0
1:00	28.5	69.2	579	21	4.8	ON	OFF	MS	ON	OFF	0
2:00	28.1	68.3	566	19	4.8	ON	OFF	MS	ON	OFF	0
3:00	27.8	67.4	564	18	4.8	ON	OFF	MS	ON	OFF	0
4:00	27.5	67.1	551	17	4.8	ON	OFF	MS	ON	OFF	0
5:00	27.2	66.8	546	16	4.8	ON	OFF	MS	ON	OFF	0
6:00	26.8	65.9	558	15	0	ON	OFF	MS	OFF	OFF	0
7:00	26.0	65.3	564	12	0	ON	OFF	MS	OFF	OFF	0

C. Results and Discussion for the Fuzzy Logic-based DC Cooling Fan Speed Controller Model

International Journal of Applied Mathematics
Volume 38 No. 11s 2025,
ISSN: 1311-1728 (printed version); ISSN: 1314-8060 (on-line version)

During testing, the Ta and RH values were retrieved from the ThingSpeak IoT platform and imported into MATLAB using the thingSpeakRead() function to evaluate the FLCFSCM response for driving eight DC brushless cooling fans (CFs). For hardware validation, a Particle Photon microcontroller was programmed to compute the crisp CFSP output, generate the corresponding PWM signal with a maximum value of 255 for the L298N motor driver, and upload the cooling fan speed (CFS) PWM signal back to the ThingSpeak cloud. The MATLAB-simulated and Particle Photon-based FLCFSCM outputs were compared in Fig. 21. According to fuzzy rule 13, with Ta = 22.4°C and RH = 67.4%, the MATLAB-simulated CFSP in Fig. 21(a) was 10%, corresponding to a PWM value of approximately 25, representing 10% of the full scale (255). At this operating point, the Particle Photon-based FLCFSCM drew 5.7 W from the inverter, as shown in Fig. 21(b).

The performance of a fuzzy logic–based DC cooling fan controller was evaluated simultaneously with a conventional ON–OFF controller over a 24-hour period under varying Ta and RH conditions. Ta ranged from 20.6°C at 09:00 to 28.2°C at 01:00, while RH varied between 58.9% at 09:00 and 71.5% at 21:00. Both controllers operated under identical environmental conditions, allowing a direct, real-time comparison. The FLCFSCM controller continuously adjusted the CFSP between 10% and 70%, resulting in a power draw of 5.6 W to 10.7 W, whereas the ON–OFF controller operated in binary mode, consuming 13.3 W when ON and 4.1 W when OFF. As shown in Fig. 22, the graph illustrated the smooth, adaptive regulation of the FLCFSCM compared with the stepwise operation of the ON–OFF controller.

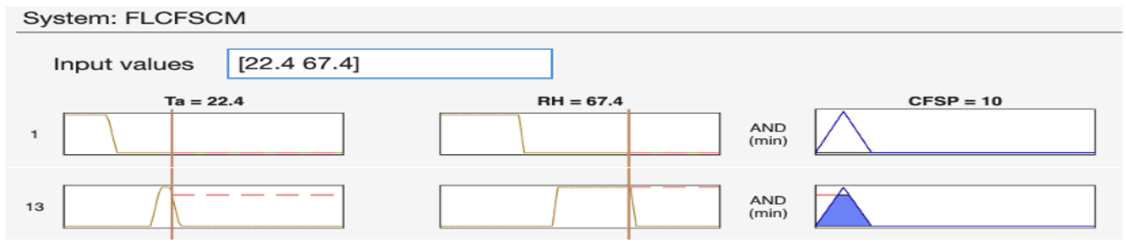

(a) MATLAB-simulated FLCFSCM crisp output

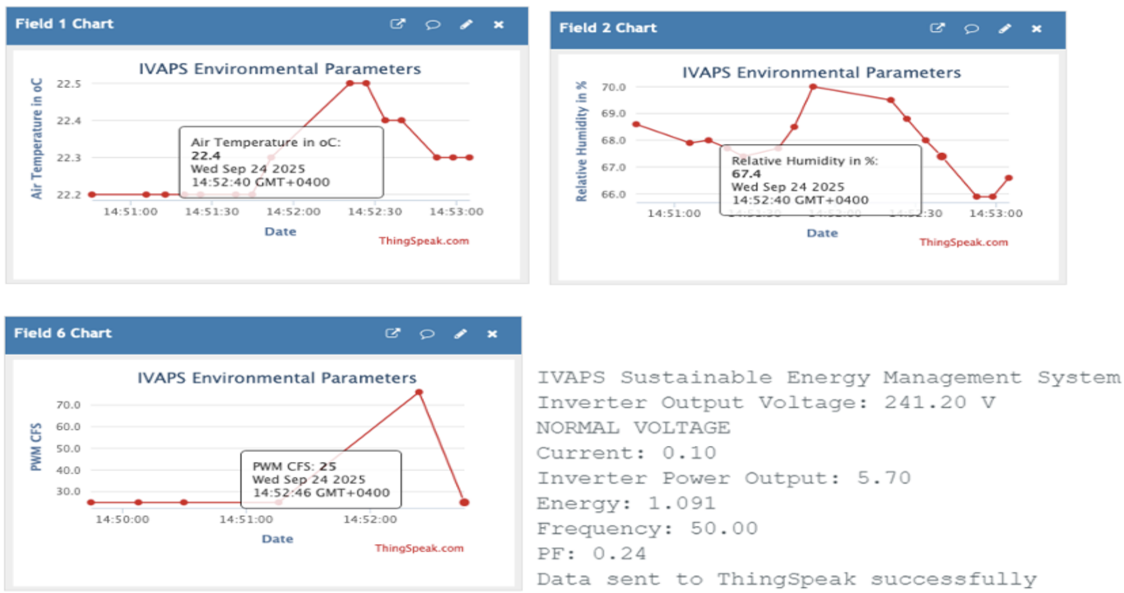

(b) Particle Photon-based FLCFSCM outputs as seen in the ThingSpeak cloud and serial monitor

Fig. 21. Comparison of the (a) MATLAB-simulated and Photon-based FLCFSCM outputs

Received: August 05, 2025

International Journal of Applied Mathematics

Volume 38 No. 11s 2025,

ISSN: 1311-1728 (printed version); ISSN: 1314-8060 (on-line version)

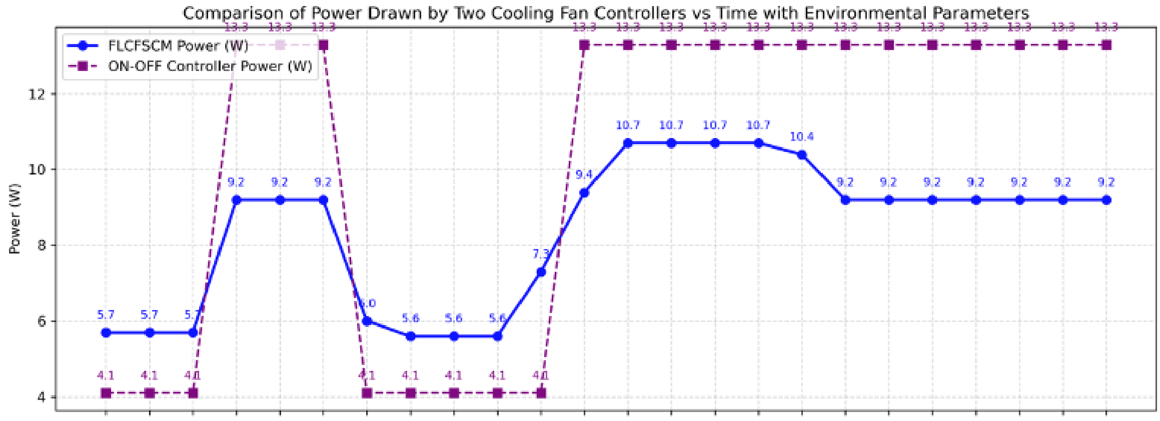

Time	8:00	9:00	10:00	11:00	12:00	13:00	14:00	15:00	16:00	17:00	18:00	19:00	20:00	21:00	22:00	23:00	0:00	1:00	2:00	3:00	4:00	5:00	6:00	7:00
Ta (°C)	21.1	20.6	22.1	22.6	22.9	22.5	22.0	21.9	21.8	21.7	23.4	24.5	25.7	26.6	27.3	27.7	28.0	28.2	28.1	27.8	27.5	27.3	26.7	26.0
RH (%)	61.0	58.9	67.5	71.2	70.8	70.3	69.1	67.8	65.9	64.2	68.2	69.3	70.8	71.5	71.2	70.8	69.9	69.0	68.3	67.4	67.1	66.9	65.9	65.3

Fig. 22. Hourly power comparison between FLCFSCM and ON-OFF CF controller

The hourly energy savings achieved by the fuzzy logic controller were computed using (19):

$$\%Power\ Saving = \frac{P_{on-off\ controller} - P_{FLCFSCM}}{P_{on-off\ controller}} * 100 \qquad (19)$$

Where: $P_{\text{ON-OFF Controller}}$ and P_{FLCFSCM} represent the instantaneous power drawn by each controller

From 11:00 to 13:00, rising Ta and RH increased the cooling demand. The FLCFSCM fan speed increased to 50% (MS), drawing 9.2 W, while the ON–OFF controller switched ON at 13.3 W. The power saving of the FLCFSCM was computed in (20) as:

$$\%Power\ Saving = \frac{13.3 - 9.2}{13.3} * 100 = 30.8\% \qquad (20)$$

Between 20:00 and 01:00, the environmental conditions peaked at 27 to 28.2 °C for Ta and 69 to 71.5% for RH. During this period, the FLCFSCM regulated the CF speed gradually between 67 and 70%, drawing 10.4 to 10.7 W from the inverter. On the other hand, the ON–OFF controller operated continuously at 13.3 W, resulting in a power saving of approximately 19.5%, as expressed in (21):

$$\%Power\ Saving = \frac{13.3 - 10.7}{13.3} * 100 = 19.5\% \qquad (21)$$

The results indicated that the FLCFSCM effectively adjusted power consumption to environmental load, thereby avoiding the overshoot and inefficiency associated with ON–OFF control [37]. The coordinated operation of both controllers showed that the variable-speed fuzzy logic CF controller delivered hourly energy savings of about 19.5% to 30.8%, with the highest efficiency occurring during moderate cooling demand. Over the full 24-hour cycle, the system saved 43.8 Wh, corresponding to a 17.8% reduction in energy consumption.

[38] reported that operating the fan at low speed in fully closed hydroponic chambers helped minimize vertical temperature and RH differences by maintaining uniform air mixing

Volume 38 No. 11s 2025,
ISSN: 1311-1728 (printed version); ISSN: 1314-8060 (on-line version)
across the canopy. Under VLS CF conditions, gas exchange was sufficient to regulate transpiration, reducing water stress and supporting steady growth. On the other hand, CF operation at full speed (100%) under ON–OFF control, compared with the FLCFSCM high-speed mode (HS, 70%), caused strong airflow, making plants lose more water and show stress symptoms like tipburn and dead tissues. Airflow velocities above 0.6 $m \cdot s^{-1}$ were shown to suppress lettuce biomass accumulation in hydroponic systems [38]. Based on the results, the FLCFSCM outperformed ON–OFF and fixed-speed fans by reducing energy consumption while maintaining optimal plant growth conditions [37], [38].

D. Results and Discussion for the Particle Photon-based Water Quality Control and Monitoring System of the IVAPS

Prior to the deployment of the Particle Photon–based Water Quality Control and Monitoring System in the IVAPS, the Atlas Scientific pH sensor was calibrated using the standard solutions provided by the manufacturer. Likewise, the Atlas Scientific conductivity K1.0 sensor was calibrated with the manufacturer's EC solution. These calibration steps ensured accurate and consistent measurements of pH, total dissolved solids (TDS), electrical conductivity (EC), and salinity (SAL) within validated ranges.

Table 9 presents the sample average 24-hour water quality data collected over one week, showing that chemical and thermal conditions remained consistently within the ranges suitable for mint cultivation. Tw varied from 21.0°C at 09:00 to a peak of 25.2°C at 22:00, due to GL operation and ambient heat. To prevent excessive heat buildup and ensure uniform nutrient distribution, the CW pump was activated between 22:00 and 00:00, keeping Tw below the hydroponic critical threshold of 35°C [13], [30]. EC and TDS gradually declined during the day as the mint plant absorbed nutrients. Nighttime dosing of nutrient solution (NS) during active GL periods increased EC and TDS.

The SAL also increased to 1 ppt at 23:00 and stayed below the 2 ppt threshold for most of the day [34]. The water pH remained stable between 6.0 and 6.2 throughout the day but dropped to a minimum of 5.4 at midnight following the addition of acidic nutrient solution. The pH-UP dispenser then raised the pH to 5.6 by 01:00, after which it stabilized around 6.0 to 6.2.

E. Results and Discussion for the Mobile Application for Monitoring and Management of IVAPS

Fig. 23 shows the environmental data from MAIVAPS, including Ta, RH, CO_2, TVOC, and LDR voltage. Fig. 24 presents the water quality parameters, such as Tw, pH, EC, TDS, and SAL, as displayed in MAIVAPS. Fig. 25 illustrates the SEMS metrics in MAIVAPS, including inverter voltage, inverter power, and battery voltage, providing comprehensive overview of the system performance and operational management. Fig. 26 shows the output of the FLCFSCM in MAIVAPS, demonstrating the reasoning behind fan speed adjustments. It highlights the environmental readings that influenced decision and identifies the specific fuzzy rules applied, providing transparency and XAI features of MAIVAPS.

Table 9. Sample weekly average 24-hour water quality data and actuator status for the IVAPS

International Journal of Applied Mathematics
Volume 38 No. 11s 2025,
ISSN: 1311-1728 (printed version); ISSN: 1314-8060 (on-line version)

Time	Water Quality Parameter Readings					Actuator status and controlled action		
	Tw (°C)	pH	EC (µS/cm)	TDS (ppm)	SAL (ppt)	NS Pump	CW Pump	pH Dispenser
8:00	21.8	6.2	1802	990	0	OFF	OFF	OFF
9:00	21.0	6.2	1797	986	0	OFF	OFF	OFF
10:00	22.2	6.1	1791	981	0	OFF	OFF	OFF
11:00	22.8	6.1	1786	976	0	OFF	OFF	OFF
12:00	23.1	6.1	1780	972	0	OFF	OFF	OFF
13:00	22.7	6.0	1776	967	0	OFF	OFF	OFF
14:00	22.2	6.0	1771	962	0	OFF	OFF	OFF
15:00	22.1	6.0	1766	957	0	OFF	OFF	OFF
16:00	22.0	6.0	1761	951	0	OFF	OFF	OFF
17:00	21.9	6.0	1725	939	0	OFF	OFF	OFF
18:00	23.9	6.0	1669	914	0	OFF	OFF	OFF
19:00	24.5	6.0	1602	875	0	OFF	OFF	OFF
20:00	25.0	6.0	1563	858	0	OFF	OFF	OFF
21:00	25.0	5.9	1536	840	0	OFF	OFF	OFF
22:00	25.2	5.9	1512	833	0	OFF	ON	OFF
23:00	25.1	5.8	1456	801	1	ON	ON	OFF
0:00	25.0	5.4	1501	825	1	OFF	ON	UP
1:00	25.0	5.6	1524	838	0	OFF	OFF	OFF
2:00	24.8	6.0	1541	847	0	OFF	OFF	OFF
3:00	24.8	6.0	1561	858	0	OFF	OFF	OFF
4:00	24.7	6.0	1601	880	0	OFF	OFF	OFF
5:00	24.7	6.0	1641	902	0	OFF	OFF	OFF
6:00	24.6	6.0	1681	924	0	OFF	OFF	OFF
7:00	24.8	6.2	1721	938	0	OFF	OFF	OFF

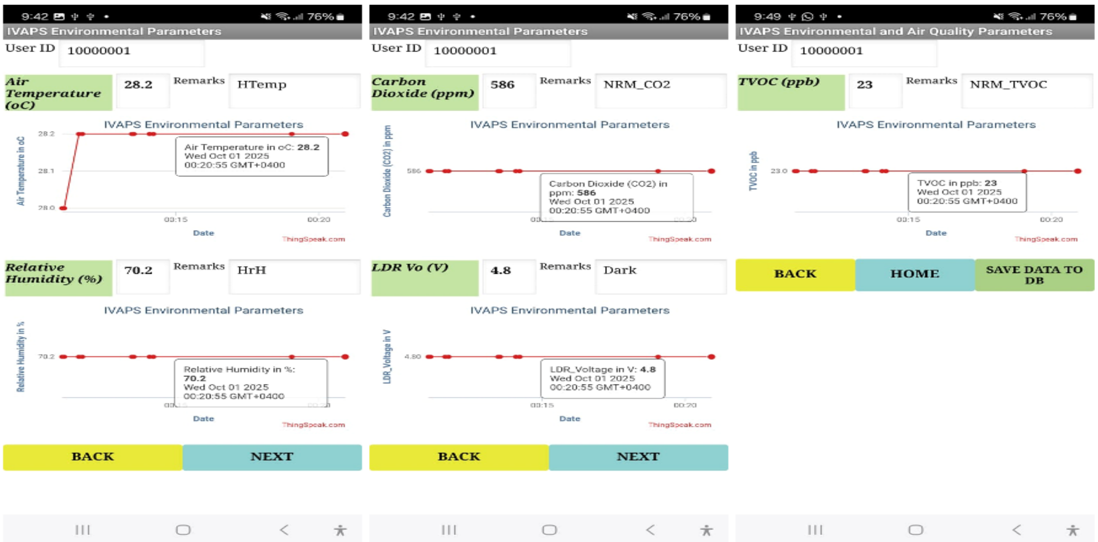

International Journal of Applied Mathematics
Volume 38 No. 11s 2025,
ISSN: 1311-1728 (printed version); ISSN: 1314-8060 (on-line version)

Fig. 23. Environmental Parameters as seen from the IVAPS mobile application

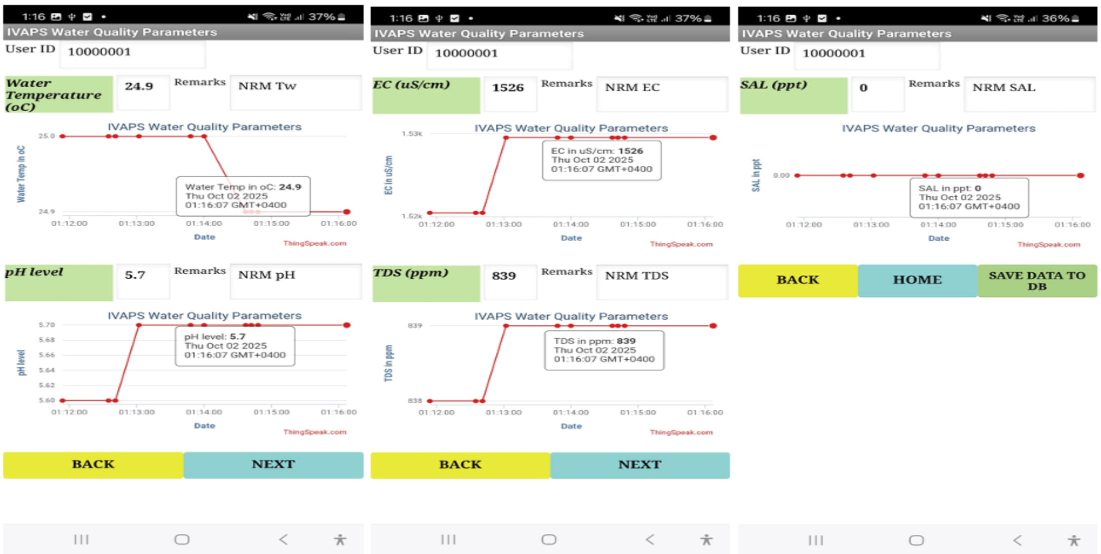

Fig. 24. Water Quality Parameters as seen from the IVAPS mobile application

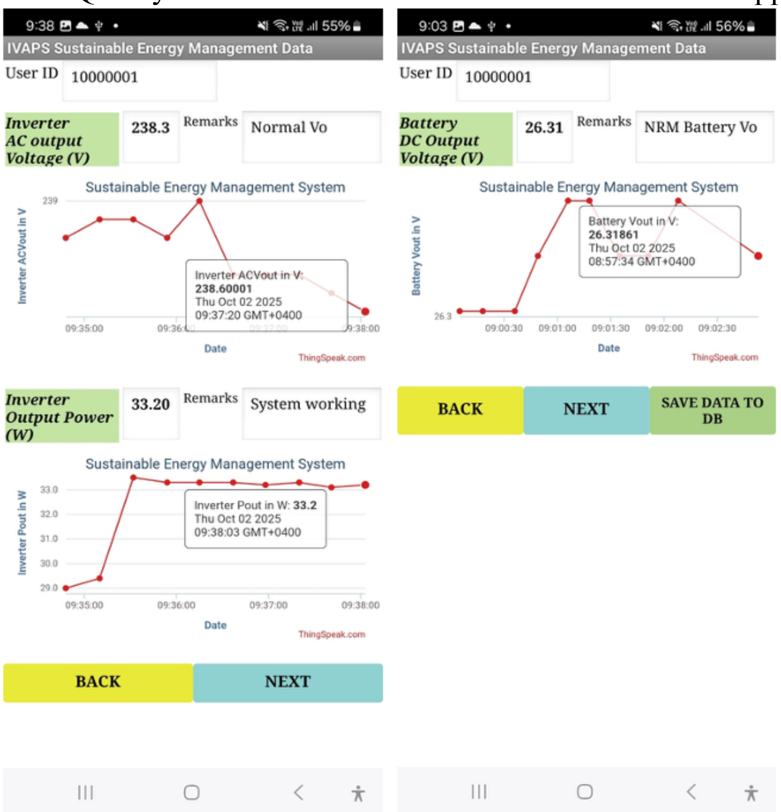

Fig. 25. SEMS Metrics as seen from the IVAPS mobile application

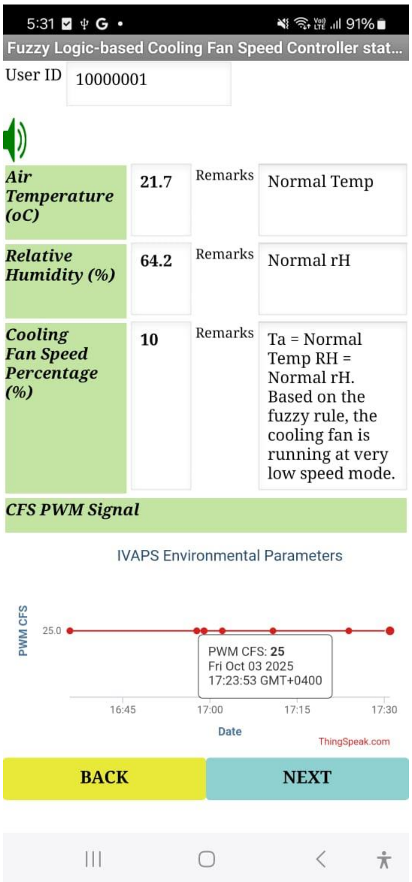

Fig. 26. CF status as seen from the IVAPS mobile application with XAI features

V. CONCLUSION

The design and implementation of IVAPS was accomplished through the use of IoT, AI and mobile technologies. The IVAPS demonstrated agricultural sustainability by precisely regulating environmental and water quality parameters within optimal ranges for mint cultivation, resulting in optimal nutrient management and crop yields. The mathematically modeled fuzzy logic-based DC fan controller adjusted to varying Ta and RH conditions, optimizing fan speed to save about 19.5% to 30.8% of energy per hour and 17.8% per day. The interactive mobile application facilitates remote monitoring of environmental and water quality indicators, as well as the status of the sustainable energy system. MAIVAPS features, such as notification alerts, rule-based XAI and text-to-speech function enhance the data visualization, improve understanding of the soilless farming system and facilitate easy navigation. Continuous data logging to the ThingSpeak cloud and database enables long-term analysis and historical performance evaluation of the IVAPS.

The recommendations to further improve the IVAPS are as follows: (a) implement an adaptive system that combines fuzzy logic with machine learning to enhance energy efficiency and environmental control; (b) develop advanced AI algorithms for comprehensive plant health assessment, which includes disease detection, growth monitoring, and stress prediction; and (c) incorporate daylight harvesting, passive cooling, and noise reduction strategies to promote green building practices and overall system sustainability.

ISSN: 1311-1728 (printed version); ISSN: 1314-8060 (on-line version)

ACKNOWLEGMENT

The authors are grateful to The Research Council of Oman for funding the research and to UTAS – Al Musanna for its continuous support. The authors also thank the technical staff and student research assistants for their help in the data collection.

REFERENCES

[1] Devesh, S., & Affendi, A. M. A. (2020). Food security dynamics in Oman: VECM approach. *Advances in Dynamical Systems and Applications*, *15*(2), 249-263.

[2] Al-Alawi, K. M. S. (2010). Food Security Approach in Sultanate of Oman. In *32nd RECA Seminar on Food Security Global Trends and Perspective, Japan: IDACA* (pp. 239-247).

[3] Farooq, M. (2022). Wheat production in Oman: experiences, challenges and opportunities. *Journal of Agricultural and Marine Sciences*, *27*(1), 1-15.

[4] Muthuraman, S., Al Haziazi, M., Uthaman, N., & Sulaiym, S. H. (2023). Sustainable food security in the sultanate of Oman. *GSC Advanced Research and Reviews*, *17*(2), 060-5.

[5] Nagayo, A. M., Mendoza, C., Vega, E., Al Izki, R. K., & Jamisola, R. S. (2017, July). An automated solar-powered aquaponics system towards agricultural sustainability in the Sultanate of Oman. In *2017 IEEE International Conference on Smart Grid and Smart Cities (ICSGSC)* (pp. 42-49). IEEE.

[6] Nagayo, A. M., Al Ghafri, H. A., Vega, E., Al Yahmadi, J. S., & Al Mujaini, M. M. (2022). Control and monitoring systems of a smart hybrid-powered integrated soil-less farming facility with a fuzzy logic-based decision support module for crop planning to enhance agricultural sustainability. *Journal of Pharmaceutical Negative Results, 13*(1), 3135–3148.

[7] Khan, S. A., Epoc, F., Al Shamsi, I. R., & Shamim, A. (2022). How far modern vertical farming is appropriate for developing countries like Oman?: A review based analysis. *Delhi Business Review*, *23*(2), 9-15.

[8] Mishra, Nikita & Hangshing, Lamneithem & Kadam, Darshan & Tapang, Tage & S., Shameena. (2024). Advances in Vertical Farming: Opportunities and Challenges. *Journal of Scientific Research and Reports*. 30. 212-222. 10.9734/jsrr/2024/v30i82241.

[9] Kuo, C. G., Chiu, C. W., & Chung, P. S. (2025). A New Approach to Expanding Interior Green Areas in Urban Buildings. *Buildings*, *15*(12), 1965.

[10] Yuan, X., Hu, J., Marcelis, L. F., Heuvelink, E., Peng, J., Yang, X., & Yang, Q. (2025). Advanced technologies in plant factories: exploring current and future economic and environmental benefits in urban horticulture. *Horticulture Research*, *12*(5), uhaf024.

[11] Llewellyn, D., & Dixon, M. (2011). 4.26 Can plants really improve indoor air quality. *Academic Press: Burlington, MA, USA*, 331-338.

[12] Bakker, J., Lugten, M., & Tenpierik, M. (2023). Applying vertical greening systems to reduce traffic noise in outdoor environments: Overview of key design parameters and research methods. *Building Acoustics*, *30*(3), 315-338.

[13] Nagayo, A. M., & Jamisola, R. S. (2017). Cloud-based wireless monitoring system and control of a smart solar-powered aquaponics greenhouse to promote sustainable agriculture and fishery in an arid region.

[14] Fadilla, R. M., Oktafiandini, N. S. D., Adha, M., Kamelia, L., Firdaus, D. F., & Akmaliyah, A. (2021, August). The Prototype of Smart Garden Fertigation System with Solar Photovoltaic System Based on IoT. In *2021 7th International Conference on Wireless and Telematics (ICWT)* (pp. 1-5). IEEE.

[15] Naser, Md, Sazia Khandoker Esha, Md Shahrear Bhuiyan, Md Jubydul Islam, Taiyeb Hasan Sakib, Ehsanul Karim, AFM Jamal Uddin, and Abu SM Mohsin. "Design of a

Smart Greenhouse Environment Monitoring and Disease Detection System." In *2023 26th International Conference on Computer and Information Technology (ICCIT)*, pp. 1-6. IEEE, 2023.

[16] Thazin, T., Aung, Z. L., & Win, T. T. (2019). IoT based hydroponic temperature and humidity control system using fuzzy logic. In *Conference: ICSE Yangon* (pp. 1-5).

[17] Ahshan, Razzaqul. (2021). Potential and Economic Analysis of Solar-to-Hydrogen Production in the Sultanate of Oman. *Sustainability*. *13*. 9516. 10.3390/su13179516.

[18] Yasa, K. A., Purbhawa, I. M., Yasa, I. M. S., Teresna, I. W., Nugroho, A., & Winardi, S. (2023). IoT-based Electrical Power Recording using ESP32 and PZEM-004T Microcontrollers. *Journal of Computer Science and Technology Studies*, *5*(4), 62-68.

[19] Venkatesh, C., Mallan, D., & Vishal, P. (2024). Hydroponics in mint. *AgriArticles*, 4(5), 924–928. Retrieved September 2, 2025, from https://agriarticles.com/wp-content/uploads/2024/10/E-04-05-279-924-928.pdf

[20] Sommano, S.R., Kanthawang, N., Janpen, C., Norkum ai, P., Wongkaew, M., Inkham, C., Van Doan, H. and Cheewangkoon, R. (2022). Physiological and Oxidative Responses of Japanese Mint Grown Under Limited Water and Nitrogen Supplies in an Evaporated Greenhouse System. *Frontiers in Sustainable Food Systems*, *5*, p.808327.

[21] Rahul, S. G., Kavitha, P., & Hemakumar, V. S. (2024, July). Monitoring Indoor Mint Crop Conditions for a Controlled Environment Using IoT. In *2024 2nd International Conference on Sustainable Computing and Smart Systems (ICSCSS)* (pp. 357-362). IEEE.

[22] Dunn, B., & Poudel, M. (2023, September). *Greenhouse carbon dioxide supplementation*. Oklahoma State University Extension. Retrieved September 2, 2025, from https://extension.okstate.edu/fact-sheets/greenhouse-carbon-dioxide-supplementation.html

[23] Burchett, M., Tarran, J., & Torpy, F. (2007, November). *Potted-plants improve indoor environmental quality: Research review and sponsorship opportunities*. Green Plants for Green Buildings. Retrieved September 2, 2025, from https://greenplantsforgreenbuildings.org/wp-content/uploads/2014/01/PottedPlantsImproveIndoorEnvironmentalQuality.pdf

[24] Fernández-Agüera, J., Dominguez-Amarillo, S., Fornaciari, M., & Orlandi, F. (2019). TVOCs and PM 2.5 in naturally ventilated homes: three case studies in a mild climate. *Sustainability*, *11*(22), 6225.

[25] Khairuddin, S. H., Hasan, M. H., Akhir, E. A. P., & Hashmani, M. A. (2022). Generating type 2 trapezoidal fuzzy membership function using genetic tuning. *Computers, Materials and Continua*, *71*(1), 717-734.

[26] Kreinovich, V., Kosheleva, O., & Shahbazova, S. N. (2020). Why triangular and trapezoid membership functions: A simple explanation. In *Recent developments in fuzzy logic and fuzzy sets: dedicated to Lotfi A. Zadeh* (pp. 25-31). Cham: Springer International Publishing.

[27] Umamaheswari, S., Preethi, A., Pravin, E., & Dhanusha, R. (2016, October). Integrating scheduled hydroponic system. In *2016 IEEE International Conference on Advances in Computer Applications (ICACA)* (pp. 333-337). IEEE.

[28] Eden Green. (2023, March 22). *Hydroponic mint guide: How to grow mint in a greenhouse*. Eden Green Technology. Retrieved September 14, 2025, from https://www.edengreen.com/blog-collection/hydroponic-mint-guide

[29] Fimbres-Acedo, Y. E., Traversari, S., Cacini, S., Costamagna, G., Ginepro, M., & Massa, D. (2022). Testing the effect of high pH and low nutrient concentration on four leafy

vegetables in hydroponics. *Agronomy*, *13*(1), 41. https://doi.org/10.3390/agronomy13010041

[30] Richa, A., Fizir, M., & Touil, S. (2021). Advanced monitoring of hydroponic solutions using ion-selective electrodes and the internet of things: a review. *Environmental Chemistry Letters*, *19*(4), 3445-3463. https://doi.org/10.1007/s10311-021-01233-8

[31] Jones Jr, J. B. (2016). *Hydroponics: a practical guide for the soilless grower*. CRC press.

[32] Stone, N. M., & Thomforde, H. K. (2004). *Understanding your fish pond water analysis report* (pp. 1-4). Cooperative Extension Program, University of Arkansas at Pine Bluff, US Department of Agriculture and County Governments Cooperating.

[33] Rusydi, A. F. (2018, February). Correlation between conductivity and total dissolved solid in various type of water: A review. In *IOP conference series: earth and environmental science* (Vol. 118, p. 012019). IOP publishing.

[34] Ghamarnia, H., Basiri, M., Ghobadi, M., & Palash, M. (2023). Performance of peppermint (Mentha piperita L.) in different water deficit and salinity management. *Agrotechniques in Industrial Crops*, *3*(2), 84-95.

[35] Ryu, D. K., Kang, S. W., Ngo, V. D., Chung, S. O., Choi, J. M., Park, S. U., & Kim, S. J. (2014). Control of temperature, humidity, and CO_2 concentration in small-sized experimental plant factory. *Acta Horticulturae, 1037,* 477–484. https://doi.org/10.17660/ActaHortic.2014.1037.59

[36] Al Jaouni, S., Saleh, A. M., Wadaan, M. A., Hozzein, W. N., Selim, S., & AbdElgawad, H. (2018). Elevated CO2 induces a global metabolic change in basil (Ocimum basilicum L.) and peppermint (Mentha piperita L.) and improves their biological activity. *Journal of plant physiology*, *224*, 121-131. [37] Abuhussain, M. A., Alotaibi, B. S., Aliero, M. S., Asif, M., Alshenaifi, M. A., & Dodo, Y. A. (2023). Adaptive HVAC system based on fuzzy controller approach. *Applied Sciences*, *13*(20), 11354.

[38] Peiró, E., Pannico, A., Colleoni, S. G., Bucchieri, L., Rouphael, Y., De Pascale, S., Paradiso, R., & Gòdia, F. (2020). Air distribution in a fully-closed higher plant growth chamber impacts crop performance of hydroponically-grown lettuce. *Frontiers in Plant Science, 11,* 537. https://www.frontiersin.org/articles/10.3389/fpls.2020.00537